TÉCNICO LISBOA

Statistical methods applied to high-pressure combustion in ESTHER facility

Jorge García-Rivas Carmona

Thesis to obtain the Master of Science Degree in

Aerospace Engineering

Supervisor(s): Dr. Maria Luis Castela

Prof. Mario Lino da Silva

Examination Committee

Chairperson:

Supervisor:

Member of the Committee:

October 2017

Resumo

No âmbito do projeto ESTHER (European Shock-Tube for High Enthalpy Research), é necessário compreender os processos que governam o fenómeno da combustão em condições extremas de pressão inicial da mistura. A instalação experimental ESTHER compreende uma câmara de combustão onde é injetada uma mistura de hidrogénio, oxigénio e hélio, inicialmente à pressão entre 30 a 100 bar. A ignição da mistura inicia-se com o auxilio de um laser infravermelho que é direcionado para o interior da câmara de combustão. Verificou-se, ao longo dos múltiplos ensaios da câmara de combustão, que o processo de ignição/combustão poderá ocorrer em regimes diferentes, dando origem tanto a eventos de detonação como a de deflagração, dependendo das condições iniciais da mistura e da configuração do sistema optico (laser). A instalação experimental ESTHER requer elevadas taxas de repetibilidade do regime de combustão e para tal, o regime de detonação devera ser evitado. Porem, durante a combustão, as pressões máximas pós ignição deverão ser o mais elevadas possível para que a razão de pressões da secção do driver dê origem a ondas de choque com velocidades de propagação superiores a 10 km/s. Por conseguinte, nesta fase de desenvolvimento do ESTHER é critico determinar quais as variáveis mais importantes e que mais impacto tem no regime e na eficiência da combustão. No entanto, apesar de critico, os processos de combustão a altas pressões não esta ainda totalmente compreendidos e os modelos analíticos e/ou simulações numéricas disponíveis na literatura referem quase na sua totalidade a casos de ignição a baixos/médios valores de pressão do gás. A compreensão dos fenómenos e das correlações entre as variáveis experimentais do ESTHER através do estudo dos resultados disponíveis na literatura torna-se, por isso, limitada.

Na presente tese a estratégia passa por usar métodos estatísticos avançados para se estabelecerem modelos empíricos da combustão a alta pressão, a partir de um conjunto de observações experimentais disponíveis na base de dados do ESTHER. Três métodos estatísticos foram implementados e analisados: Regressão Logística Multivariada, Redes Neuronais e a Analise de Componentes Principais. A analise estatística mostra a correlação entre as diferentes variáveis independentes do sistema, sublinhando as diferenças entre cada método estatístico. Os resultados obtidos permitem uma melhor compreensão do processo de combustão a altas pressões, mostrando que o sistema optico e a diluição por hélio são duas das variáveis que mais afetam o regime de combustão. Por fim, o programa desenvolvido no âmbito desta tese, onde as ferramentas estatísticas são alimentadas pela base de dados do ESTHER, ira servir como ferramenta de apoio a decisão nos futuros ensaios do ESTHER. A capacidade de previsão do algoritmo será cada vez mais robusta à medida que a base de dados vai aumentando com o numero de ensaios. Neste sentido, o trabalho desenvolvido nesta tese é um primeiro passo para o uso de técnicas avançadas de machine learning em problemas complexos, como o da combustão experimental.

Palavras-chave: Combustão a alta pressão, Regressão Logística Multivariada, Redes Neuronais, Analise de Componentes Principais, ESTHER, combustão experimental, machine learning.

Abstract

In the framework of ESTHER (European Shock-Tube for High-Enthalpy Research) project, the understanding of the processes that govern the combustion under extreme conditions of initial gas pressure is necessary. The ESTHER facility includes a combustion chamber where a H_2/O_2/He mixture is pumped, at initial pressure between 30 and 100 bar. An infrared laser pointed to the vessel triggers the mixture ignition. Along exhaustive test campaigns, it has been found that different ignition regimes involving both detonation and deflagration events may occur depending on the mixture initial conditions and the optical system configuration (laser). ESTHER facility requires high combustion repeatability rates and hence detonation regime must be avoided. However, during combustion, the maximum pressure should be as high as possible so the pressure ratio in this driver section induce a shock wave with propagation speeds exceeding 10 km/s. Therefore, it is critical to determine which variables are most important and which have the most impact on the combustion regime and combustion efficiency. However, although critical, high pressure combustion processes are yet to be fully understood and the analytical models and/or numerical simulations available in the literature refer almost entirely to cases of ignition at low/medium gas pressures. Awareness of ESTHER combustion and correlations between the considered ESTHER variables through the study of the available results is therefore limited.

In the present thesis, the strategy adopted is to use advanced statistical methods to establish empirical models of the high-pressure combustion, using a set of experiments available in ESTHER database. Three statistical methods were analysed and implemented: Multivariate Logistic Regression, Neural Networks and Principal Component Analysis. The statistical analysis shows the correlation between the different variables of the system, highlighting the difference between methods. The results obtained provide a better understanding of the combustion process at high pressures, showing that the optical system and the helium dilution are two of the variables that most affect the combustion regime. Lastly, the program developed under the scope of this thesis, where statistical tools are fed by the ESTHER database, will serve as a decision support tool in future ESTHER trials. The predictive capacity of the algorithm will be increasingly robust as the database increase with the number of ESTHER experiments. In this sense, the work developed in this thesis is a first step to the use of advanced techniques of machine learning in complex problems, such as experimental combustion.

Keywords: High-pressure combustion, Multivariate Logistic Regression, Neural Networks, Principal Component Analysis, ESTHER, experimental combustion, machine learning.

Contents

Resumo . . . iii
Abstract . . . v
List of Tables . . . ix
List of Figures . . . xi
Nomenclature . . . 1
Glossary . . . 1

1 Introduction **1**
1.1 Motivation . . . 1
1.2 Objectives . . . 2
1.3 Thesis Outline . . . 3

2 Review of the Statistical Methods **5**
2.1 Mutivariate Logistic Regression . . . 7
2.2 Neural Networks . . . 8
2.3 Principal Component Analysis . . . 10
2.4 Practical Example . . . 12

3 Statistical analysis of combustion phenomena at high-pressure conditions **15**
3.1 Brief description of the ESTHER study . . . 15
3.2 Characterisation of the Experimental Variables . . . 16
3.2.1 Independent Variables . . . 16
3.2.2 Dependent Variables . . . 21
3.3 Algorithms and Implementation . . . 24
3.3.1 Variables Normalization . . . 25
3.3.2 Multivariate Logistic Regression . . . 25
3.3.3 Neural Network . . . 26
3.3.4 PCA . . . 34

4 Results **37**
4.1 Ignition Regime results . . . 38
4.1.1 MLR . . . 38

4.1.2 Neural Network . . . 41
4.2 Pressure ratio results . . . 46
4.2.1 MLR . . . 46
4.2.2 Neural Network . . . 48
4.3 Consumption velocity results . . . 53
4.3.1 MLR . . . 53
4.3.2 Neural Network . . . 54
4.4 PCA . . . 54
4.4.1 Dimension reduction . . . 55
4.4.2 Data clustering . . . 56

5 Conclusions **59**
5.1 Future Work . . . 61

Bibliography **63**

A H_2/O_2 reaction mechanism **67**

B Weights matrices used in Chapter 4 **71**
B.1 Ignition regime matrices . . . 71
B.2 Pressure ratio matrices . . . 72

List of Tables

2.1 Truth table of function OR 12
2.2 Truth table of function XNOR 13

4.1 Normalization parameters. 37
4.2 MLR coefficients for dependent variables Detonation. 39
4.3 MLR coefficients for dependent variable Dual Slope. 40
4.4 Ignition regime probability distribution regarding the ignition source. 41
4.5 MLR results for the dependent variable pressure ratio. 47
4.6 MLR results for the dependent variable consumption velocity. 53

B.1 Weight matrix $\Theta^{(1)}$ used in Section 4.1. 71
B.2 Weight matrix $\Theta^{(2)}$ used in Section 4.1. 72
B.3 Weight matrix $\Theta^{(1)}$ used in Section 4.2. 72
B.4 Weight matrix $\Theta^{(2)}$ used in Section 4.2. 72

List of Figures

2.1 Sigmoid function. 7
2.2 Neural network structure. 9
2.3 PCA performance simplification. 11
2.4 OR function as a MLR regression. 12
2.5 XNOR function as a neural network. 13

3.1 ESTHER shock tube. From left to right: combustion chamber, compression tube, shock-tube and dump tank. 15
3.2 Initial temperature record. 17
3.3 Initial pressure record. 17
3.4 Equivalence ratio record. 19
3.5 Helium dilution record 20
3.6 Ignition source record. 20
3.7 Pressure-time curve recovered after shot #155. 21
3.8 Pressure ratio record. 22
3.9 Ignition regime record. 22
3.10 Detonation record. 23
3.11 Dual slope record. 23
3.12 Consumption velocity record. 24
3.13 Pressure-time curve recovered after shot #150. 24
3.14 Neural network schematics. 27
3.15 Effect of the regularization factor, considering a) $\lambda = 0$ (Overfitting) and b) $\lambda = 100$ (Underfitting). 29
3.16 Errors vs. regularization factor. 32
3.17 Cost function vs. number of iterations. 33
3.18 Cost function vs. number of units in the second layer. 33
3.19 K-means algorithm clustering process. 34
3.20 PCA dimension reduction. 35

4.1 Ignition regime probability distribution regarding T_0, conditioned by (a) without lens and (b) lens. 42

4.2 Ignition regime probability distribution regarding p_0, conditioned by (a) without lens and (b) lens. . . . 43
4.3 Ignition regime probability distribution regarding ϕ, conditioned by (a) without lens and (b) lens. . . . 44
4.4 Ignition regime probability distribution regarding dil, conditioned by (a) without lens and (b) lens. . . . 45
4.5 Discretization of the dependent variable pressure ratio. . . . 48
4.6 Pressure ratio probability distribution regarding T_0, conditioned by (a) without lens and (b) lens. . . . 49
4.7 Pressure ratio probability distribution regarding p_0, conditioned by (a) without lens and (b) lens. . . . 50
4.8 Pressure ratio probability distribution regarding ϕ, conditioned by (a) without lens and (b) lens. . . . 51
4.9 Pressure ratio probability distribution regarding dil, conditioned by (a) without lens and (b) lens. . . . 52
4.10 Comparison between the original initial temperature and the projected initial temperature. 55
4.11 Comparison between the original lens and the projected lens. . . . 55
4.12 Reduction of the combustion dimensional space. . . . 56
4.13 Data clusters found by the algorithm, differentiated by colors. . . . 56

Chapter 1

Introduction

The development of new combustion technologies, as for instance ram/scramjets and pollutants-free hydrogen-oxygen combustion engines, requires new insights on the ignition phenomena at specific mixture conditions. In ram/scramjets, flow velocity at the entrance of the combustion chamber can easily reach values significantly higher than that of turbulent flame velocity, leading to unstable flames and misfire events. Mixture ignition is, therefore, extremely challenging for those stringent flow conditions. Hydrogen can help reduce mixture ignition delay and stabilise flames that otherwise would not be stable. The use of hydrogen as fuel in ground power generation is also regarded as one of the solutions to face pollutants emission, since water is the only product of hydrogen-oxygen combustion. However, safety hazards in duct systems and the explosive nature of hydrogen-oxygen mixtures still pose significant technical challenges. The dilution of H_2/O_2 mixtures by inert gases such as helium, is one of the solutions to avoid explosive events. Yet, the ignition and propagation of premixed H_2/O_2/He flames at very high-pressure conditions, similar to those found inside aeronautical engines or ground energy generation technologies, is still poorly understood. Theoretical and several modelling strategies are used to understand the phenomena, yet the process is very complex and difficult to capture numerically and theoretically. As it will be discussed throughout this manuscript, new original strategies can be successfully applied to predict ignition regimes even when theory and modelling are still not capable of fully describing ignition at high pressure conditions or are too computationally expensive.

1.1 Motivation

The work developed in this thesis was motivated by the need of accurately predict the combustion regimes inside the combustion driver section of the new European Shock-Tube for High Enthalpy Research (ESTHER) facility of the European Space Agency (ESA). This facility is under final stage commissioning at IPFN/IST, and opens new perspectives regarding the study of combustion at high pressure conditions. A prototype of the final ESTHER combustion chamber was initially constructed to qualify both the gas filling system and the driver mechanical design, and nowadays is being used to study in more detail deflagration and detonation regimes of H_2/O_2/He mixtures at gas filling pressures up to 100

bar. The whole ESTHER facility gathers multiple processes but the focus in the present study is the combustion phenomena. Typical input parameters of the experiment are: *Initial gas filling pressure, O_2, H_2 and He mole fractions, the ignition source and rest time of the mixture*, among others. After igniting the mixture, a piezoelectric sensor captures the temporal evolution of the gas pressure inside the combustion chamber. This single experimental output, pressure-time curves, can be closely correlated to the combustion process and useful information regarding ignition delay, detonation and tulip flames phenomena among others can be obtained.

The construction of this prototype and the test campaigns carried out by the Hypersonic Plasmas Laboratory (HPL) group ensure the access to a large number of experiments, referred herein after as "shots", that can be studied statistically. Indeed, as some combustion phenomena can be directly deduced from the pressure-time curve, today the experimental data available at HPL presents a rich opportunity to statistically study the combustion phenomena. The point here is to use the available data from the shots to estimate the probability of a given event. Thus, the relationship between inputs and outputs could lead to the understanding of the physics behind. Each one of these shots costs hundreds of euros to be performed. Moreover, if the experimental parameters lead to a detonation regime, some critical parts such as combustion chamber windows (through which the laser beam enters the chamber/vessel) can be compromised, increasing even further the cost of the shot. Although detonation is highly undesirable for this kind of applications, it becomes important from a statistical standpoint, as it helps design a robust statistical combustion model to describe the process.

It is, therefore, of major interest to predict the shot outcome regarding safety hazards for all the range of the experimental input parameters of ESTHER. This will help understand the physics and design combustion experiments at high pressure conditions as well as save money and time. The approach adopted in this work is original and have never been implemented systematically. Combustion is a multi-physics phenomena gathering hundreds or thousands of chemical reactions, energy transfer to and from the surroundings and thermodynamic balances between the atomic species. The process is highly complex and has a certain randomness. At such high gas temperatures and pressures, and with turbulence and shock waves generated during the process, the system becomes rapidly chaotic inside the combustion chamber. A consequence of this chaos is that, for several shots with the same input parameters, different results are obtained. This fact leads us to the present project. The strategy is to bring statistics to this problem, constructing a powerful tool to predict the randomness of the system.

1.2 Objectives

Today, statistical methods such as Neural Networks, Multivariate Logistic Regression and Principal Component Analysis methods challenge modelling and simulation status, being some of them, part of the modelling strategy itself.

The statistical approach is the bone marrow of the present work. The objectives of the present work can be described as follows:

- Development of a numerical framework to perform a statistical analysis of the ESTHER shots,

considering the following methods:

  - Multivariate Logistic Regression;
  - Neural Networks;
  - Principal Component Analysis.

- Perform statistical analysis of the ESTHER shots data, available at the Hypersonic Plasmas Laboratory;
- Identify important parameters governing combustion at high pressure conditions typically found in ESTHER, by extracting meaningful physics out of the statistical study.

1.3 Thesis Outline

The thesis is organized in five chapters of which the present one provides the introduction, motivation and the scope of this work.

In the second chapter, named Statistical methods, the experimental setup and measurement techniques, including uncertainties of the experimental procedure, are described from a theoretical standpoint.

The third chapter, Statistical Analysis of Combustion Phenomena at High-Pressure conditions, presents the implementation of the methods described in the previous chapter. The methods are applied to the case of study.

Chapter 4 will analyse the results of the methods described on the second and third chapter, as well as interpretate the physical and statistical meaning of the results.

Finally, chapter 5 summarizes the main conclusions of this manuscript and lists a set of suggestions for future research.

Chapter 2

Review of the Statistical Methods

Although ESTHER combustion chamber was projected to operate in deflagration mode, detonation cannot be considered an unprobable event after being triggered by several shots in ESTHER. Whereas detonation is an odd phenomenon in the majority of practical applications of hydrogen, its behavior under extreme conditions such as high initial pressure are still poorly known. Thus, it is important to determine at which conditions detonations are likely to happen in order to prevent the destructive impact of detonation phenomena.

Hydrogen combustion is known by its sensitivity to detonation. Even so, its properties as ”clean” gas make it adequate for many applications, with the purpose of mitigating atmospherical pollution. In order to deal with such a hazardous character and avoid undesired detonations in combustion chambers and storage tanks, the conditions that favor this detonations has been studied during the past years. Ng *et al.* [1] used a detailed chemical kinetics model to meassure the effects of elevated initial pressure (up to 10 atm) on detonation sensitivity, showing that beyond a critical pressure of 4 atm, the hydrogen-air mixture becomes less sensitive to the increase of the gas pressure. As shown by Cicarrelli *et al.* [2], the sensitivity to detonation of a hydrogen-air mixture increase with mixture temperature in the range 300K-650K. Kratzel *et al.* [3] developed a numerical model for detonation propagation. Besides detonation, is known that the flame after ignition eventually evolves into a tulip-shaped flame, event that changes velocity and pressure evolution during the combustion, in a phenomena called dual slope. The formation of these flames begins with the reduction of the flame area caused by the flame quench at the sidewalls of the vessel. These flames involve gas recirculation and changes in the mixture local velocity, which translate in sudden changes in the burn velocity. This change alters the pressure rise ratio, which is reflected in the pressure-time curves as changes in the slope. Detailed information of these tulip flames and their formation and propagation mechanisms can be found in Combustion Phenomena [4]. Xiao *et. al* [5] found that normal and distorted tulip flames can be produced in absence of wall friction yet the boundary layer has certain effect in the flame dynamics. Xiao *et. al* [5] concluded that further investigations are needed, including a more accurate flame propagation model.

In this work just few examples about hydrogen combustion research are provided. Yet, although literature is full of investigations about different aspects of hydrogen combustion, all of them recognize

the lack of data in both extreme conditions and multi-physics combustion models. Combustion science moves towards a multi-physics model that fits all the empirical data obtained after non practical combustions such as high pressure combustion or laser-triggered combustion, for being the future of propulsion engineering and energy sources. In this frame, this research will try to clarify some aspects of hydrogen/oxygen combustion at very high gas pressures, as found in ESTHER experiments.

As stated before, this combustion regime is a very complex and is still poorly understood. In order to understand such a multiphysics and complex phenomena, three different metodologies can be used:

Analytical solution: The analytical solution of a multiphysics problem requires that the real configuration of the experiment is completely described, in order to take into account all the details that can affect the outcome. In ignition phenomena, flame kernel generation through an external source of energy, the flame front propagation, unburnt gas mixture circulation and interaction with side walls among other phenomena must be taken into account to fully capture the combustion processes. Therefore, in order to address any problem, drastic simplifications are usually required. The physics of a multi-physics combustion are really difficult to capture, so it can be concluded that whereas analytical solutions can be succesfully applied to canonical and academic problems, it is not an adequate solution to accurately capture the physics underlying the ESTHER combustion phenomena.

Numerical simulation: This method requires simplified models and computational development of the problem. The set of Navier-Stokes equations and species balance equations must be solved to perfectly model a combustion process. Particularly, this model aims for the coupled solution of the following equations or system of equations:

- Continuity equation
- Momentum equation
- Energy equation
- Species balances

Although H_2O is the only product of H_2/O_2 combustion, several species such as H, O, OH, HO_2 and H_2O_2 are intrinsic to the process. Therefore, modelling the combustion can become computationally expensive. A typical kinetic scheme of H_2/O_2 mixture, developed by Li *et al.* [6], is given in Appendix A.

Statistical solution: This solution refers to the use of experimental/real data to predict the results of new experiments. Advanced statistics techniques and algorithms can be used in our favor to classify experimental onsets. The main advantage of this method is that, while it does not solve any physical equation, it uses the data from previous experiments to derive empirical correlations.

Many authors have used statistical approach to address science-related problems, from medicine, for instance, Albalak *et al.* [7]; to engineering. Combustion itself has been studied using these methods

many times, either for turbulent flow characterization (Bennett *et al.* [8]) or emissions prediction (Traver *et al.* [9]). Within these statistical methods, we can find a wide variety of tools that could be useful for analyzing any problem, being one of the tasks of the investigator selecting the most adequate.

As stated before, statistical methods use the data that is already available from previous experiments to establish the correlation between the system variables and the system outcome. Being so, they don't rely on a physical equation or model, but those physics underlying the problem can be inferred from the results of the statistical analysis, in a numerical approach.

After a preliminary analysis of the ESTHER experiments, and a survey of the state-of-the-art, the statistical methods Multivariate Logistic Regression and Neural Networks were found to be the most interesting tools. Both methods will be complemented with Principal Component Analysis, statistical method widely used in combustion field.

Consequently, three methods will be used in the present work: Multivariate Logistic Regression, Neural Networks and Principal Component Analysis. The three methods are described briefly in the following sections.

2.1 Mutivariate Logistic Regression

Mutivariate Logistic Regression (MLR) has been widely used during the past years in statistical studies such as malignant/cancerous cells detection [10] or demographic analysis [11], among other topics. In engineering, MLR is mainly used in probabilistic approaches, and hence, a tool to translate any discrete result into a probability continuum becomes necessary. The function widely used through the literature is the *sigmoid function*, $g(x)$, given as follows,

$$g(x) = \frac{e^x}{1 + e^x} \tag{2.1}$$

where x is the argument of the function.

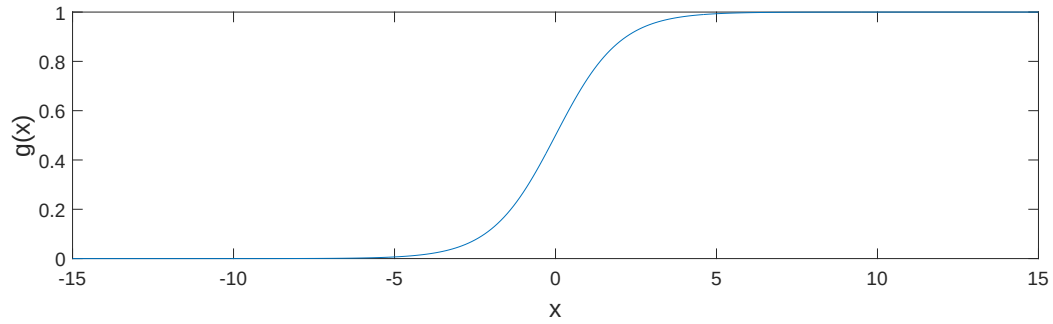

Figure 2.1: Sigmoid function.

This sigmoid function is a special form of the logistic function. It is capable of returning a value within the probability interval ([0, 1]) regardless the argument x, as long as it is a real number. Moreover, it has the property of changing from zero to one and vice versa in a narrow domain ([-5,5]), which makes

it adequate for probability studies.

MLR tries to infer the x in Eq. (2.1) by assigning a coefficient to each variable involved in the problem, so if the increase of certain variable (x_i) favors the event to happen, $g(x)$ increases as well. Thus, the goal of this method is to assign values to the coefficients in the regression equation, so the influence of each variable is reflected. This regression equation is given by Eq. (2.2),

$$Y = \theta_0 + \theta_1 X_1 + \theta_2 X_2 + ... + \theta_p X_p \tag{2.2}$$

where p represents the number of X variables in the problem and $\theta_{i=1,...,p}$ are the coefficients associated to each variable. θ_0 is the *intercept term*, and represents the outcome when no information about the system is given, this is, the presumable outcome. As shown in Eq. (2.2), the influence of the variables is linear. Yet, the model can be adapted to include non linear relationships by including different powers of the variables, if needed.

Thus, MLR solves $g(Y) = P(x)$, where x is the phenomenon which probability we want to calculate. $P(x)$ is therefore given by:

$$P(x) = \frac{e^{\theta_0+\theta_1 X_1+\theta_2 X_2+...+\theta_p X_p}}{1 + e^{\theta_0+\theta_1 X_1+\theta_2 X_2+...+\theta_p X_p}} \tag{2.3}$$

Equation (2.3) provides the probability of the phenomenon x. The sigmoid function translates negative outputs into desfavorable probabilities and positive values translate into high probabilities. It is therefore important to normalize the features sample in order to get zero mean. When the value of $P(x)$ is less than 50%, the result is desfavorable, whereas for $P(x) > 50\%$, the result is considered favorable.

As stated before, MLR is used for probability estimations, since the result of the regression is always a value within the interval [0, 1]. Therefore, dichotomous variables, which represent absolute events (something that either happens or not, as a detonation) are predicted using this method. Conversely, for continuous variables, such as physical magnitudes, Multivariate Linear Regression is used. The difference between them remains in the use of the sigmoid function. Prescinding from it, the result of the regression belongs to the whole domain of real numbers, so this method can be used to measure variables like velocity or pressure.

Some examples of MLR applied to combustion field can be found in Meng *et al.* [12] and Wang *et al.* [13], who used this technique to study and measure CO_2 emissions and furnace combustion state, respectively, with succesful results.

2.2 Neural Networks

A neural network is a very powerful state-of-the-art tool in statistical analysis, which is starting to be widely used for a lot of different applications, setting the base of the so-called machine learning, branch of technology dedicated to make the computers capable of learning and improving. Examples of how technology evolves around these neural networks are face recognition algorithms (Rowley *et al.* [14]), spam classifying (Chuan *et al.* [15]), computer virus detection (Tesauro *et al.* [16]) and autonomous

navigation (Pomerlau [17]), among others. The hitech neural networks tool is gaining importance in the 21^{st} century as part of our society, accompanying technology as it evolves.

Neural networks can be roughly described as many MLR concatenated and linked between them, capable of building stronger links between the provided variables in order to predict the result with high level of accuracy. A neural network is a black box, receiving the variables involved and returning the result, as they create a map of weights/coefficients that can be analysed to get the influence of the different variables in the problem. Figure 2.2 illustrates a common neural network structure.

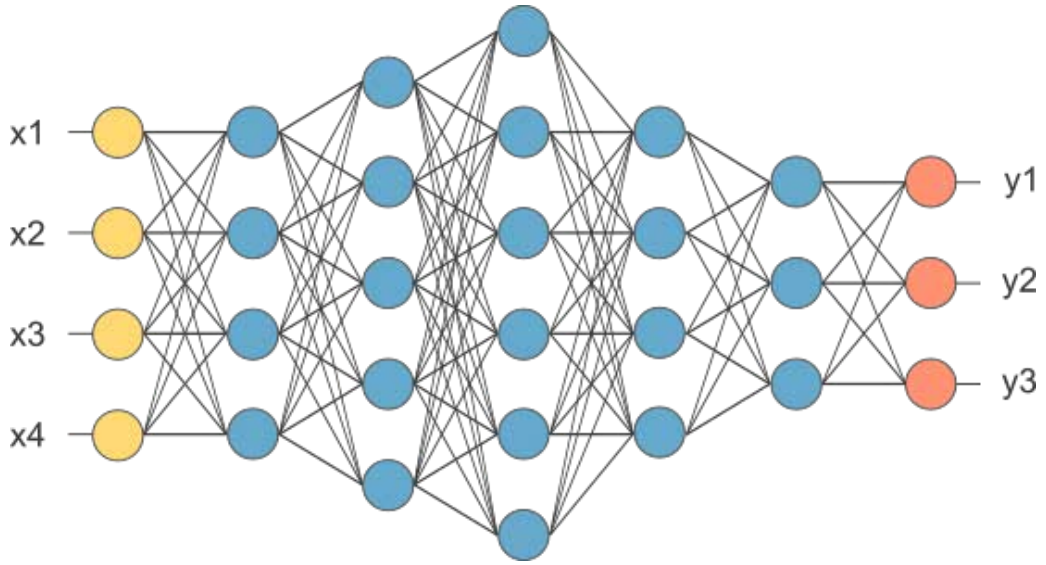

Figure 2.2: Neural network structure.

In Fig.2.2, x1, x2, x3 and x4 (nodes in yellow) represent the different features or independent variables of the problem whereas y1, y2 and y3 represent the outcome or dependent variables (nodes in red). Both sets form the input and output layer, respectively. The nodes in blue are called hidden units or activation units, because of their capacity to switch from zero to one in a reduced interval, thanks to the use of the sigmoid function. These activation units are organized in hidden layers (columns in Fig. 2.2). In Fig. 2.2, five hidden layers are represented.

Each single activation unit results from a Multivariate Logistic Regression, in which it was considered that the variables are all the units in the previous layer, so their value also remain within the interval [0, 1]. Thus, in the example of Fig. 2.2, every node in the output layer is the result of a MLR using the three nodes in the fifth hidden layer as input variables. Note that this is a multiclass classification problem, i.e. there is more than one output, so the neural network must estimate the probability of belonging to any of these classes, being all of them dichotomous variables.

As can be seen, this method is capable of establishing more complex relationships between variables. It is computationally more expensive than the MLR, but, by far, more useful for complex problems. The neural network needs a sample of experiments to learn from. Provided this sample (in this work, ESTHER shots), the neural network creates the coefficients matrices needed to fit the dimensional requirements of the problem. Once the network has been trained, this set of matrices of weights, $\Theta^{(l)}$

(where l represents the number of frontiers between layers, six in Fig. 2.2), with similar meaning to the θ_i seen in MLR (Section 2.1), is set up. The study of these matrices could reveal how combustion works regarding some of its ignition regimes, in addition to show the relevance of the initial parameters in the combustion result.

Tosun *et al.* [18] compared Logistic Regression and Neural Networks methods in internal combustion diesel engine performances, concluding that the latter offers more accurate predictions for all the parameters considered. He also remarked the time and expenses savings that can be achieved with the use of these neural networks. A similar study was carried out by Pino-Mejías *et al.* [19], who used both methods to predict energy consumption, energy demand and CO_2 emissions in Santiago, Chile. The conclusions of this study also showed that Neural Networks method offers greater precision in the predictions than regression methods. This research highlighted the fact that, the larger the database, the better the performance offered by the network. Indeed, the number of training examples is a factor that sets the behavior of the algorithm; it must be large enough.

As many other authors of recent studies, Tosun [18] and Pino-Mejías [19] agree in the potential that these statistical algorithms have in the future of propulsion and energy engineering. Nevertheless, application of neural networks in engineering is a developing field and yet to be fully implemented. Algorithms similar to Neural Networks have been studied and applied to combustion for the past years. An example is found in the work of Vaughan *et al.* [20], who used Extreme Learning Machine (technique close to Neural Networks) to map a near chaotic combustion behavior.

It is now clear how the use of these algorithms will benefit the determination of ESTHER combustion. Indeed, Neural Networks will be the principal statistical method in this project, to better understand high-pressure combustion and to determine the multi-physics behavior of laser induced combustion and the phenomena involved.

2.3 Principal Component Analysis

Principal Component Analysis (PCA) is a very useful method that differs a bit from the other two presented above. PCA is classified as unsupervised/blind methods, while MLR and Neural Networks are supervised statistical methods. The difference remains in the outcome, unknown for *unsupervised learning*. Supervised algorithms train with labeled data (the outcome is known), whereas unsupervised algorithms do not. Hence, there is no way to evaluate the accuracy in the results of these methods, since the true output of the problem is unkown a priori.

PCA application as statistical method in this work passes by its combination with the K-means algorithm. This algorithm has the capacity of clustering, i.e. classifying the data regarding its initial variables, without taking into account the output. The goal is to correlate the labels created by K-means algorithm with the actual results obtained after the ESTHER experiments. It will also help to check the relevance of the problem's variables, but as the problem does not have many variables, the dimension reduction is limited. K-means algorithm was successfully used by Perini [21] to cluster high-dimensional combustion chemistry datasets.

PCA aims to diminish the complexity of the problem by reducing the order of the dimensional space, i.e. the number of variables involved. The dimension reduction can also be used in a preliminary step for MLR or Neural Networks analysis with large number of variables. It helps neglect possible non important variables that have been selected as significant a priori, as well as eliminate redundancy.

The dimension reduction is achieved by extracting the eigenvectors from the covariance matrix, which contains the covariance of all the variables considered. These variables must be previously normalized in order to get unit eigenvectors. Once these vectors are known, PCA performs a series of projections into lower dimensional spaces, reducing the dimensional order of the problem. A simplification of its performance is shown in Fig. 2.3, where PC1 and PC2 refer to the two principal components of the example's variables dataset.

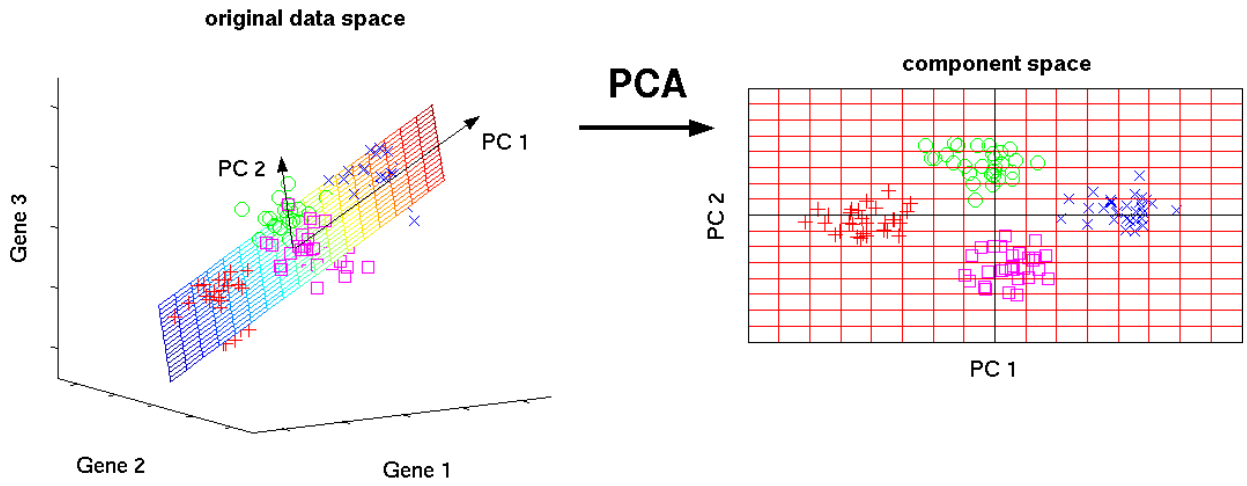

Figure 2.3: PCA performance simplification.

PCA has been widely used in combustion field to model reduced basis for high dimensional combustions, as seen in Shuterland *et al.* [22]. Thus, PCA is often used to reduce complex multiphysics combustion simulations, such as the transport equation system or the involved species balance. These reduced models enable detailed multidimensional simulations that otherwise would be CPU limited. Other applications of PCA in combustion can be found in the researchs of Isaac *et al.*[23], who studied the effect of using a reduced base for the estimation of source terms in a transport combustion model; Mirgolbabaei *et al.* [24], who proposed a PCA-based approach to advance the thermo-chemical state of the mixture in one-dimensional turbulence; and Owoyele *et al.*[25], who demonstrated the performance of principal components (most relevant variables) transport for the direct numerical simulation of a combustion problem. These authors applied PCA dimension reduction to highly complex problems, which involved many variables. This method was found a great ally to face such problems, in which the number of dimensions makes really difficult to evaluate the dependencies existing between variables involved.

In the present study, PCA method will help to clarify the physics returned by the supervised algorithms MLR and Neural Networks. However, the dimension reduction is not likely to be applied, due to the reduced number of variables of this problem. This will be described in details in Chapter 3. Even so, PCA is to be used for demonstrate the independence between variables and, hence, ensure that all of

them are statistically relevant.

2.4 Practical Example

A simple example is now proposed to better understand the different performance of MLR and Neural Networks.

As hypothetical situation, let's think about the logical function OR, which has two inputs, $X1$ and $X2$. The output of the function must return a logical one whether any of inputs is a logical one. This function can be recreated as an MLR regression if the adequate coefficients are selected, as shown in the Fig. 2.4:

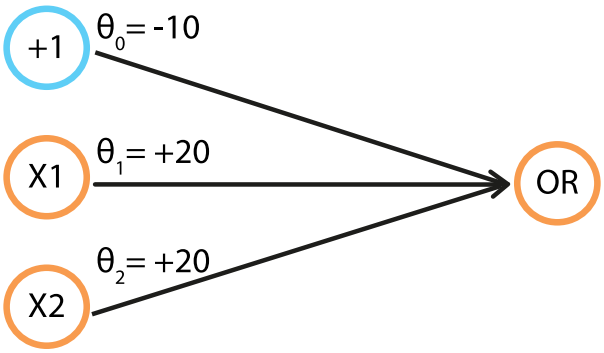

Figure 2.4: OR function as a MLR regression.

The corresponding regression equation is given by Eq. (2.4):

$$OR = g(x) = g(-10 + 10X1 + 10X2) \tag{2.4}$$

This regression fits perfectly the truth table of the logical function, which is already known (Table 2.1). In this case, both MLR and Neural Networks offer the same result, being MLR quite simpler and user-friendly than a complex neural network.

X1	X2	x	OR
0	0	-10	0
1	0	10	1
0	1	10	1
1	1	30	1

Table 2.1: Truth table of function OR

Now, let's do the same exercise with a slighty more complex function, the logical function XNOR. This function, similar to the previous function OR, must return a logical one whether both inputs equal, regardless the value (either zero or one). It can be easily demonstrated that this function can not be modelled as a MLR regression. Therefore, a more complex method must be used. Using a simple neural network, with three layers, the function requirements can be fulfilled, as indicated in Fig. 2.5.

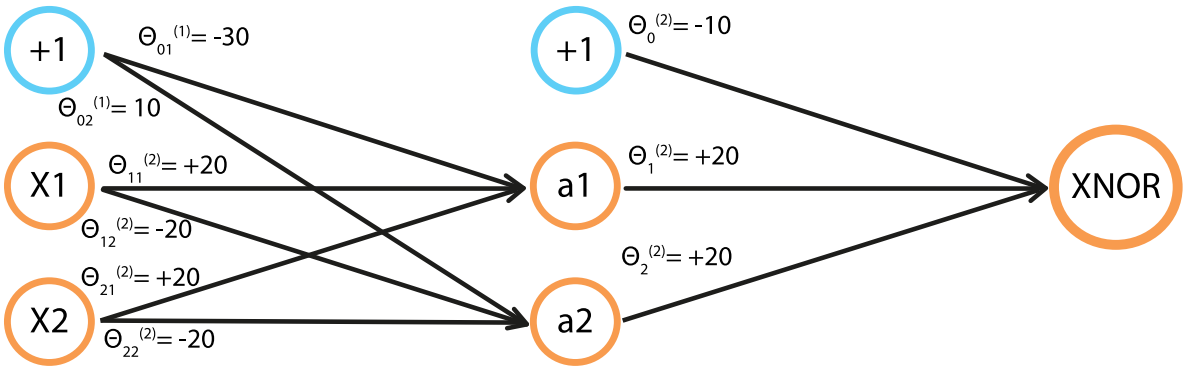

Figure 2.5: XNOR function as a neural network.

As can be seen, the truth table returned by the map in Fig. 2.5, Table 2.2, matches the desired function.

X1	X2	a1	a2	XNOR
0	0	0	1	1
1	0	0	0	0
0	1	0	0	0
1	1	1	0	1

Table 2.2: Truth table of function XNOR

Notice from the table that MLR has been applied twice, once per layer. The goal of this example is to illustrate the subtle difference between the performance of these two statistical methods. While MLR is simpler and easier, Neural Networks is capable of mapping many more links between variables, and those combinations and posibilities are really adequate to deal with unknown problems a priori.

Chapter 3

Statistical analysis of combustion phenomena at high-pressure conditions

3.1 Brief description of the ESTHER study

Fig. 3.1 presents the ESTHER shock-tube.

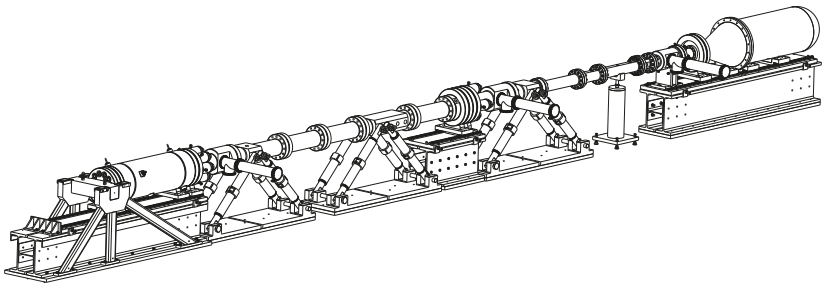

Figure 3.1: ESTHER shock tube. From left to right: combustion chamber, compression tube, shock-tube and dump tank.

The whole ESTHER experiment involves many processes and studies, yet this work focuses on the driver combustion section. The combustion takes place in a conventional combustion chamber where the H_2, O_2 and He are pumped in. Once the mixture becomes homogeneous inside the combustion chamber, a laser provides the energy needed to trigger the ignition of the mixture. The pressure rise is meant to burst a diaphragm that connects the chamber with an intermediate compression tube, filled with helium. This compression tube is connected to the shock-tube test section through a second diaphragm that will also burst when reached by the shock wave. Pressure sensor stations are placed along this section to capture the temporal evolution of the shock wave inside the tube. At the end of the shock tube

section, a dump tank recovers the H_2O resulting from the combustion process and any gas steam flow. A complete description of the system and experimental setup can be found in Lino da Silva *et al.* 2016 [26].

ESTHER facility is a relatively new experimental setup, and so far the experimental campaign includes around 180 shots. This sample offers a large number of data regarding the combustion, however one should be cautious on the selection of variables that will be part of the statistical analysis. Therefore, a first step is to evaluate the problem variables and to try to reduce the complexity of the system.

The experimental data is composed by a series of variables, some of them considered independent, also called inputs or features, and others considered dependent or outputs. The independent variables are called in such way because they are set by the ESTHER team before performing the shot and are, presumably, independent between them. The dependent variables are the outcome of the experiments and, hence, are influenced by the independent variables. The goal of the statistical analysis to be performed in this work is to correlate these two sets of independent and dependent variables.

The sets of variables available in the ESTHER database are:

Independent variables: shot ID, ambient pressure, ambient temperature, initial temperature, O_2 moles, H_2 moles, He moles, equivalence ratio, chamber pressure, initial gas pressure, dilution and ignition source.

Dependent variables: final pressure, pressure ratio, ignition regime and consumption velocity.

3.2 Characterisation of the Experimental Variables

The first step to understand ESTHER experiment is to analyze the variables involved. The main difference between the two sets of variables described above is that independent variables are set by the researchers, as inputs of the experiments, whereas dependent variables are the outcome of the experiment, meaning that they are completely unknown until the experiment has been performed. The statistical analysis aims at predicting these dependent variables, in order to increase experimental efficiency and to develop physical models that will hopefully mimic the results observed in high-pressure ignition experiments of ESTHER facility.

3.2.1 Independent Variables

- Shot ID (id). This number identifies a particular shot within the sample of the experimental shots performed in ESTHER facility. This variable is of a ranking type and therefore, has no influence on the experimental results. Shot ID variable starts in shot #124 because the 123 previous shots were conducted using a hot wire as ignition source and were also performed to qualify the gas filling system. Therefore, shots #1 to #123 are not taken into account in the statistical analysis.

- Ambient temperature (T_{amb}). The temperature in the laboratory where ESTHER experiment is

held. It depends on local environment conditions, and may influence the experimental results. Therefore, this variable is an independent variable, even though not being imposed directly by the experimentalists. It is also considered that the gas temperature inside the combustion chamber at the beginning of the shot (T_0) is equal to this ambient temperature.

The records of the initial temperature, T_0, are presented in Fig. 3.2.

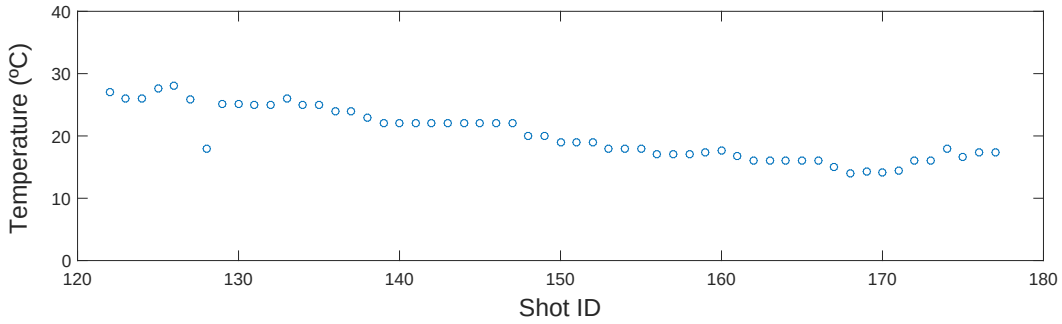

Figure 3.2: Initial temperature record.

Figure 3.2 shows that the ambient temperature variates between 14 ºC and 28 ºC, with a descending pattern along shots. The influence of this variable is not clear, and even could be considered constant or irrelevant in a first analysis. Nevertheless, it will be taken into account.

- Initial gas pressure (p_0). The gas pressure inside the combustion chamber. This variable is directly controlled by the pumping system and, hence, controlled by the research team. This pressure takes into account the ambient pressure (p_{amb}). This is the second independent variable considered in the statistical analysis.

  Pressure records are presented in Fig. 3.3.

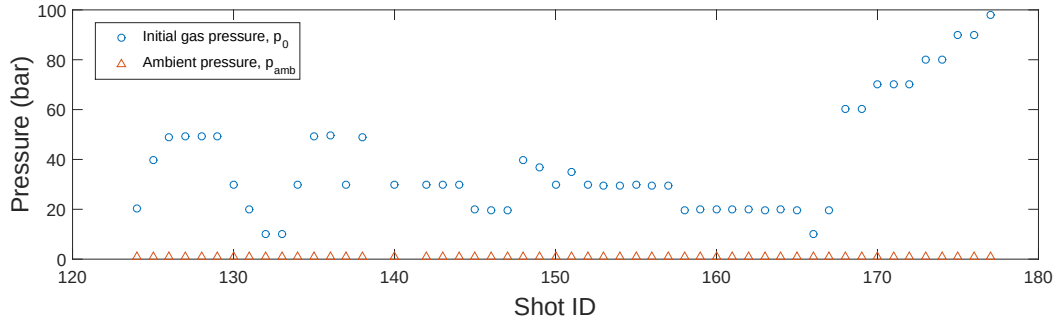

Figure 3.3: Initial pressure record.

The initial gas pressure value is therefore given by Eq. (3.1),

$$p_0 = p_{ch} + p_{amb} \tag{3.1}$$

where p_{ch} is the gas filling pressure (set at the begining of the experiment) and p_{amb} is the ambient pressure.

- Ambient pressure (p_{amb}). The pressure in the laboratory where ESTHER experiment is held. The ambient pressure varied between 1,003 bar and 1,029 bar. As shown in Fig. 3.3, this small variation on the pressure is negligible compared with the inital gas pressure set to the shots. Therefore, this variable is not considered in the statistical study.

- O_2 moles (n_{O_2}). Amount of oxygen in the gas mixture. Oxygen was selected instead of air as oxidant for the combustion reaction because the nitrogen present in the air was undesirable. A mixture of hydrogen/air was avoided by the team since the presence of N_2 would decrease the efficiency of the combustion by decreasing the final temperature of the mixture, leading to lower pressure peaks and shock wave velocities.

  This quantity is constant, as stated by Eq. (3.2),

  $$n_{O_2} = 1 \tag{3.2}$$

  and therefore it can be neglected as feature since a constant variable does not contribute any information to a statistical study.

- H_2 moles (n_{H_2}). Amount of hydrogen in the gas mixture. Because of the pressure ratio and gas sound speed ratio needed between the driver and driven sections, a hot and light gas was favorable. This made hydrogen the best suited combustible for ESTHER shock-tube. However, the explosive nature of hydrogen/oxygen mixture combustion easily leads to detonation of the mixture (see section 3.2.2). Because of this, the H_2/O_2 mixture is diluted by the inert gas helium.

  This variable is not constant, and is not related with any other variable so far, so it is the third independent variable.

- Equivalence ratio (ϕ). By definition, the equivalence ratio of a mixture is given by Eq. (3.3),

  $$\phi = \frac{n_{fuel}/n_{air}}{\left(\frac{n_{fuel}}{n_{air}}\right)_{st}} \tag{3.3}$$

  where the subindex st refers to the stoichiometric mixture.

  Moreover, the hydrogen/oxygen global combustion reaction is:

  $$2H_2 + O_2 \rightarrow 2H_2O \tag{3.4}$$

  or,

  $$H_2 + \frac{1}{2}O_2 \rightarrow H_2O \tag{3.5}$$

  Therefore, from Eq. (3.5) and Eq. (3.3), it is known that the equivalence ratio is given by:

  $$\phi = \frac{n_{H_2}}{2n_{O_2}} \tag{3.6}$$

  and thus, $\phi = \phi(n_{H_2})$.

It is not necessary to use both number of hydrogen moles and mixture equivalence ratio in this study, because, given that O_2 is a constant quantity, both are directly proportional. Equivalence ratio will be used instead the number of moles of H_2.

The equivalence ratio record is shown is Fig. 3.4.

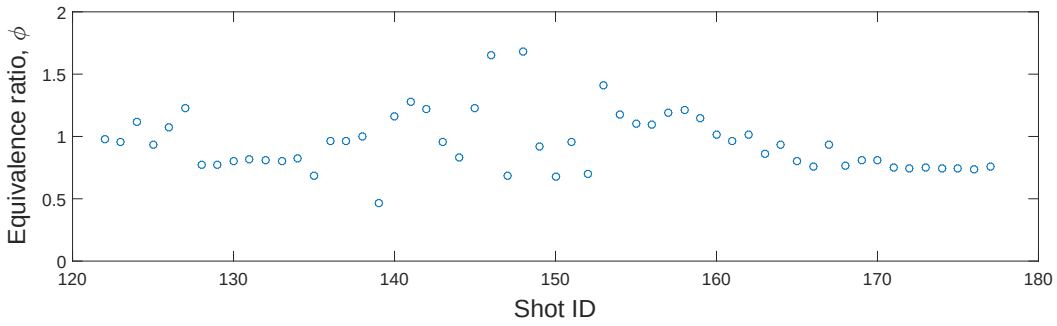

Figure 3.4: Equivalence ratio record.

As shown in Fig. 3.4, the equivalence ratio varied within the interval [0,45, 1,7], where most shots are around the stoichiometric ratio ($\phi = 1$). Nevertheless, in average, the equivalence ratio is lower than the stoichiometric ratio ($\phi < 1$).

- He moles (n_{He}). Amount of helium in the gas mixture. Helium is necessary to absorb heat from the hydrogen/oxygen combustion and to avoid high risks of detonations. Moreover, as He is an inert gas, it does not react with fuel or oxidant and it does not generates any pollution nor waste in the chamber.

  Again, this variable is not related with any other variable so far, so it will be the fourth independent variable.

- Dilution (dil). This dilution variable makes reference to the amount of diluent gas, helium, within the total mixture. It is defined as:

$$dil = \frac{n_{He}}{n_{total}} = \frac{n_{He}}{n_{O_2} + n_{H_2} + n_{He}} \tag{3.7}$$

  As $n_{O_2} = 1$ and n_{H_2} can be substituted by the equivalence ratio, the mixture dilution can be given by:

$$dil = dil(\phi, n_{He}) \tag{3.8}$$

  As stated before, equivalence ratio (ϕ) is one of our independent variables, and therefore it is included in the analysis. Due to this, the amount of helium automatically fits Eq. (3.7), so this variable can substitute He moles as fourth independent variable. Figure 3.5 shows the records of helium dilution in ESTHER shots.

  Indeed, dilution factor was a key feature at the time of designing the chamber, as explained in Castela *et al.* 2017 [27]. It is known that detonation will always occur for helium dilution factors below 60% but, conversely, above 75% no ignition will be triggered. It is important to note that

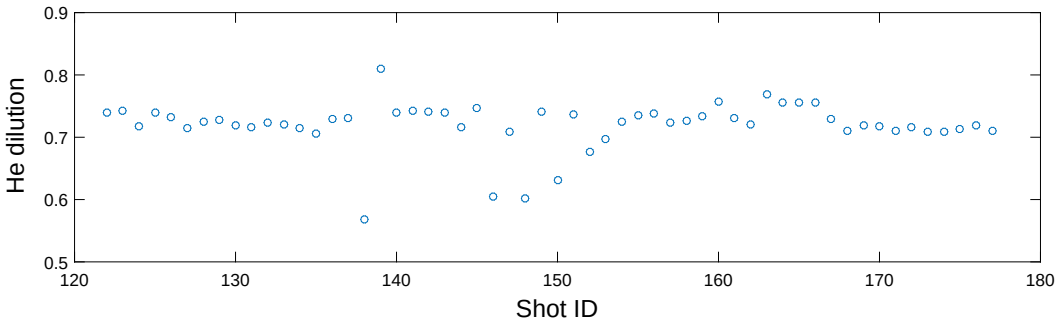

Figure 3.5: Helium dilution record

these thresholds were observed in experiments using the laser ignition source. In fact, it was observed that these limits would be wider in case of hot wire ignition source.

- Ignition source. This discrete variable, of posible values 1, 2, 3 and 4, represents the method of ignition used, either hot wire (1, full wire, or 2, half wire) or laser (3, without lens, or 4, with lens). The record of ignition sources used during ESTHER experiments is shown in Fig. 3.6.

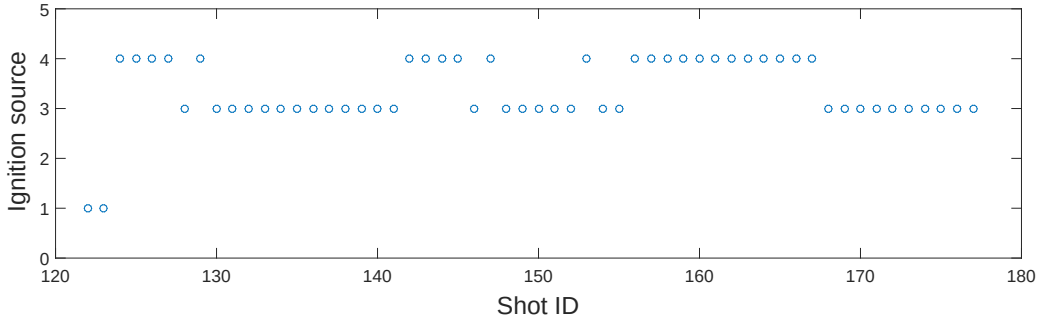

Figure 3.6: Ignition source record.

The statistical study no longer takes into account the hot wire as ignition source, as it was used only twice in the experimental campaign. Therefore, shots #122 and #123 would not contribute with any statistically relevant information and could even worsen the performance of the statistical methods.

Only laser ignition source is considered, where a Q-switch Quantel Brilliant Nd:YAG laser is pointed to the chamber from one of its ends. Then, it enters the vessel through a fused silica window providing energy to the mixture. This laser can operate under two different configurations. If the laser beam enters the chamber without focalization, the energy gradient that the laser transmits to the mixture is wide and soft. Conversely, if a special lens is assembled before the window, the laser is focalized onto one point. Therefore, the energy gradient transmitted is narrower and sharper.

Consequently, from now on, this variable will be referred as Lens ($lens$). This Lens is a dichotomous variable (it values either zero or one): $lens$ = 0 means that the shot was performed without lens, whereas $lens$ = 1 means that the laser was focalized with lens.

This variable is not related to any other variable described above and, therefore, it is the fifth

independent variable.

Summarizing, the set of independent variables has been reduced to:

Independent variables: T_0, p_0, ϕ, dil, $lens$

3.2.2 Dependent Variables

- Maximum pressure (p_{max}). It refers to the maximum gas pressure (pressure peak) reached after the ignition. It is a direct measure of the experiment, and so a dependent variable. The evolution of pressure over time is the only data recovered after the shots, so every possible result must be extracted from the pressure-time curve. An example of this curve, corresponding to shot #155, is shown in Fig. 3.7.

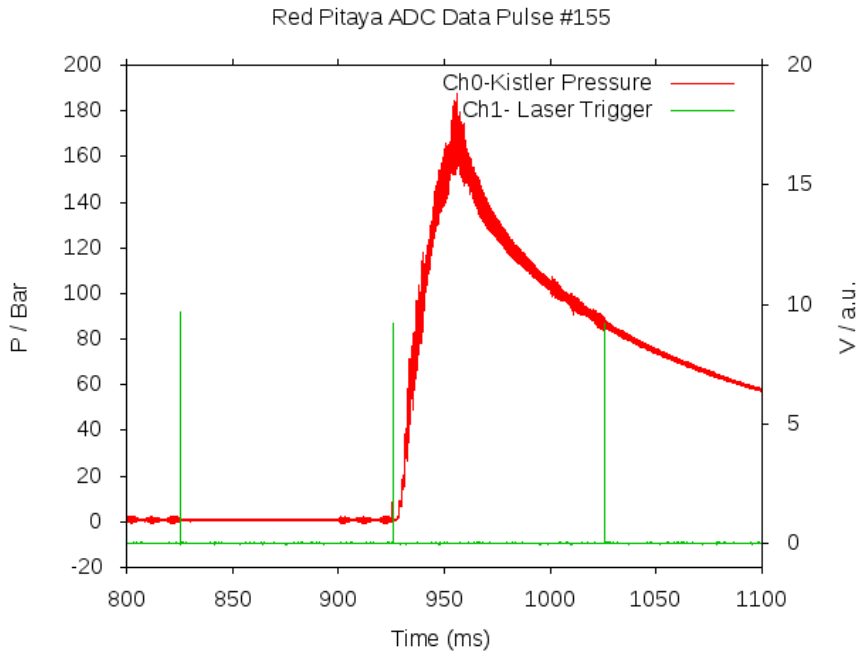

Figure 3.7: Pressure-time curve recovered after shot #155.

As explained, all the data used in this statistical study is available at the ESTHER facility database. After each shot, a curve like the one presented in Fig. 3.7 is generated and, from it, other dependent variables can be inferred.

- Pressure ratio (p_{ratio}). The pressure ratio stands for the ratio between the maximum and initial value of the gas pressure. By definition:

$$p_{ratio} = \frac{p_{max}}{p_0} \tag{3.9}$$

Figure 3.8 illustrates the records of pressure ratio.

Then, as done with the independent variables, this ratio will substitute the final pressure as dependent variable. Being intrinsically related, there is no point in performing a statistical study for both

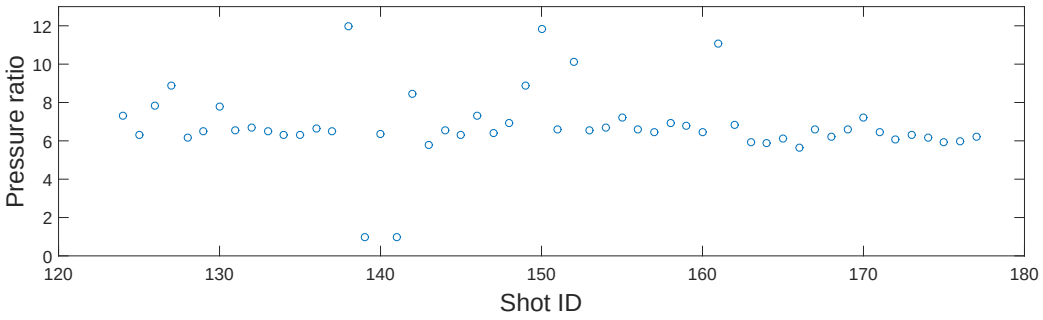

Figure 3.8: Pressure ratio record.

variables. Hence, pressure ratio one is more interesting from the predictions standpoint.

- Ignition regime. This dependent variable is the most important in this study. The ignition regime is represented by discrete values to describe the combustion phenomena occurring at each shot; 1: single slope deflagration; 2: dual slope deflagration; 3: single slope detonation; 4: dual slope detonation. The events of ignition regime for each shot are shown in the Fig. 3.9.

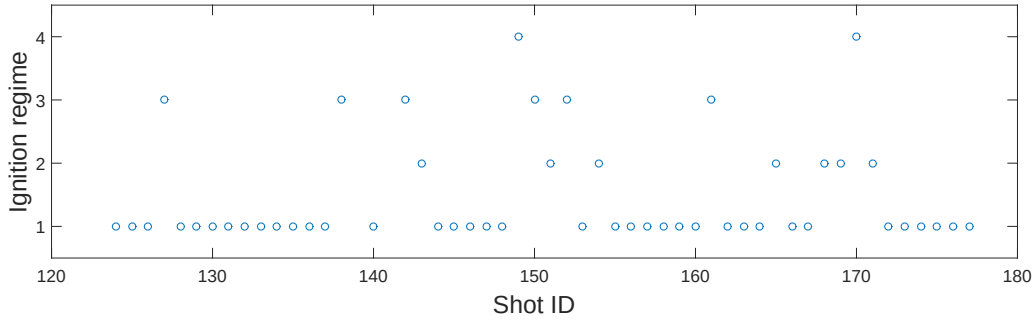

Figure 3.9: Ignition regime record.

Basically, two phenomena can be identified regarding the ignition regime. The first is the detonation (or the absent of it) and the second is the dual slope (or the absent of it). Detonation occurs when the flame front velocity reaches sonic conditions. If this flame front velocity is subsonic, ignition is associated with a deflagration. The dual slope curve is related to tulip flames phenomena, as reported by Dunn-Rankin *et al.* [28] in a series of high-speed schlieren photographies. This phenomenon can be recognized in the pressure-time curve, where the pressure rise would present two different slopes. This inflection in the pressure evolution is explained by a rapid decrease of the flame area that accompanies the flame quench at the sidewalls of the combustion vessel, as explined by Dunn-Rankin.

Therefore, it is interesting the study of the dual slope and detonation phenomena separately, to establish the factors that trigger them. This study could reveal some link between both phenomena. In order to do so, two different variables are created: Detonation and Dual Slope. These variables are dichotomous variables, i.e. represent absolute phenomena: either happened or didn't. Thus, a zero means that the phenomenon did not occur, meaning a one the opposite. Both are plotted

in Figs. 3.10 and 3.11, respectively.

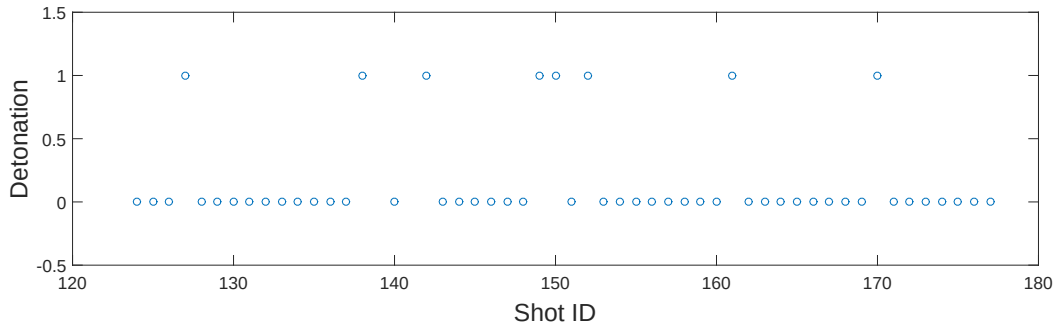

Figure 3.10: Detonation record.

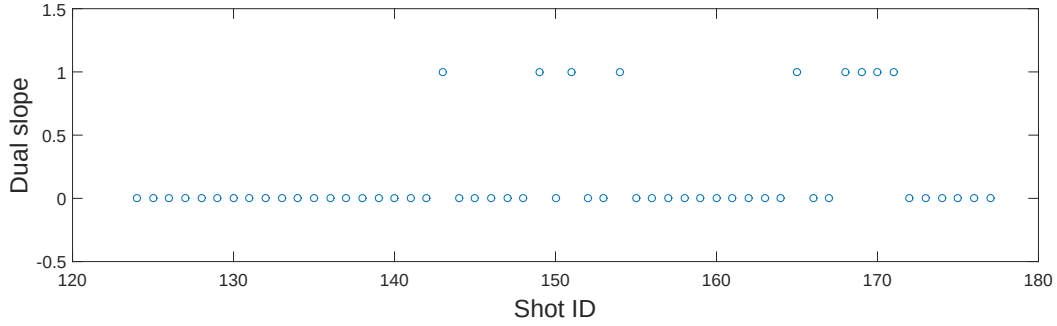

Figure 3.11: Dual slope record.

As shown in Figs 3.10 and 3.11, detonation and dual slope are not statistically common events. Even when its characterization is utterly important, detonation regime must be avoided.

- Consumption velocity (v_{ch}). This variable represents the gas consumption velocity. It is defined in terms of the length of the combustion chamber (l_{ch}) and the elapsed time between initial and maximum gas pressure (Δt_{ig}). This variable is given by Eq. (3.10).

$$v_{ch} = \frac{l_{ch}}{\Delta t_{ig}} \tag{3.10}$$

In the previous expression, $l_{ch} = 0,6$ m. The records of the consumption velocity can be seen in Fig. 3.12.

Figure 3.13 shows the pressure-time curve of shot #150, which was excluded of the plot shown in Fig. 3.12 for returning an abnormally high consumption velocity.

Indeed, this anomalic pulse returned the highest pressure ratio whitin the sample (p_{ratio} = 11,8) and produced a strong detonation. The comparison of its pressure-time curve with the one in Fig. 3.7 shows that this detonation is way more stronger than the deflagration of shot #155. Even so, it is considered an isolate case since similar shots did not produce such powerful ignitions.

Therefore, consumption velocity is the last dependent variable to be included in the statistical analysis.

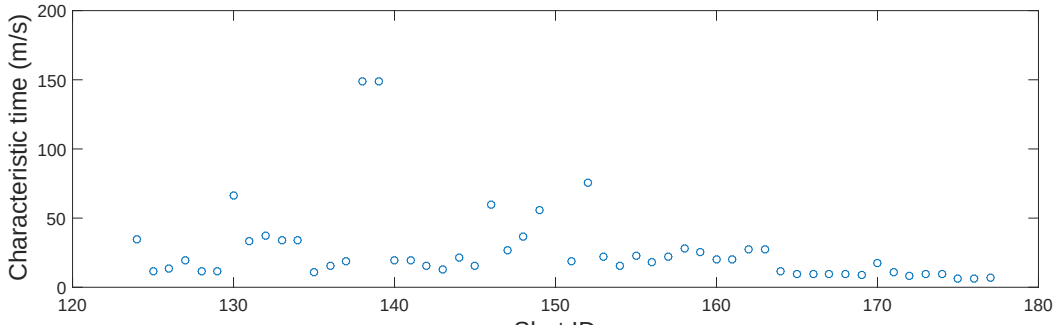

Figure 3.12: Consumption velocity record.

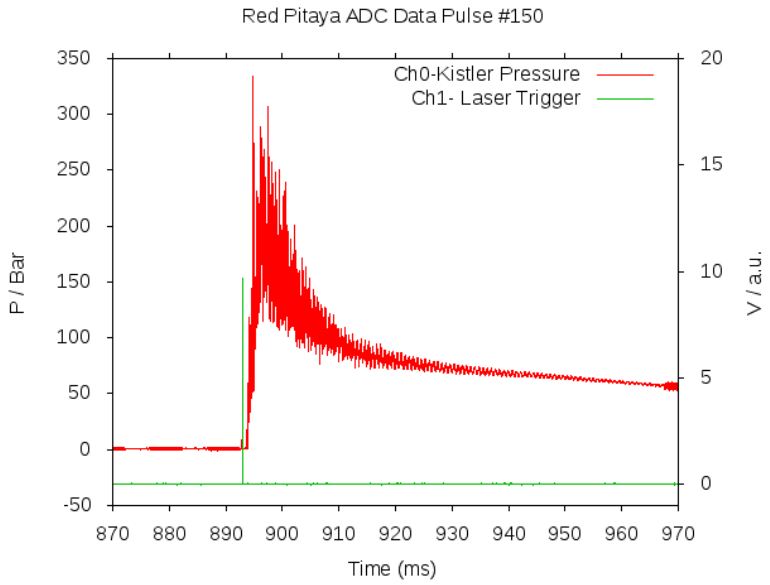

Figure 3.13: Pressure-time curve recovered after shot #150.

To sumarize, the dependent variables are the following,

Dependent variables: p_{ratio}, $Ignition\ regime$ ($Detonation$, $DualSlope$), v_{ch}

and the intended correlation is given by:

$$p_{ratio},\ Ignition\ regime,\ v_{ch} = f(T_0,\ \phi,\ p_0,\ dil,\ lens$$

3.3 Algorithms and Implementation

The implementation of the statistical methods, as well as the development of the algorithms, was based on *Machine Learning*, by Ng [29]. This course served as a guideline to correctly develop this phase of the project, yet some changes were needed in order to adapt the methods and algorithms to the combustion problem.

The programming language chosen to hold the algorithms is MATLAB, version R2015a, following the recommendations of Ng [29]. This language is very intuitive and user-friendly for statistical analysis, and it was preferred over more sophisticated languages, like Python or C++, because of its simplicity. It is highly recommended to use MATLAB or Octave, which is free software, for developing the statistical

algorithms. Once fully developed, they can be translated into another language.

In this section, the main development milestones and algorithms routines are explained. Chapther 4 contains the results of this implementation.

3.3.1 Variables Normalization

Although MLR and Neural Networks would work with raw data for both independent and dependent variables, is proven that they may diverge, or just not reach convergence, if the scales of the independent variables are very different among them. On the other hand, PCA requires the data to be normalized to select the right principal components. MLR analysis will benefit of this operation as well as the neural network, improving their performance.

So, in order to set all the variables in the same order of magnitude, the first step is to apply *feature scaling*, given by Eq. (3.11),

$$\bar{x}_i = x_i - \mu_i \tag{3.11}$$

where μ_i represents the mean average value of each of the x_i independent variables.

Now, performing *mean normalization*, the goal is to make the variables to have approximately zero mean.

$$\hat{x}_i = \frac{\bar{x}_i}{x_{i_{max}} - x_{i_{min}}} \tag{3.12}$$

Once mean normalization has been applied, the range of values of the variables is reduced to [-1, 1] and the average value of the variable will be close to zero. In Eq. (3.12), similar results can be obtained replacing the denominator with the statisical deviance of the variables, σ_i.

After this implementation, the algorithms will work faster and more efficiently. For the sake of simplicity, the accent from the normalized variables will be omitted onwards, being all the independent variables normalized ($\hat{x} \rightarrow x$).

3.3.2 Multivariate Logistic Regression

MLR is a supervised statistical method that aims to model the probability of the dependent variables to happen, in case they are dichotomous or discrete, and to return an absolute value, if the dependent variable is a continuous magnitude, using Multivariate Linear Regression.

The starting point is the so called independent variables vector, x_i, which is composed by all the x_{ij} independent variables described in section 3.2.1: initial temperature, initial gas pressure, equivalence ratio, helium dilution and ignition source. Considering all the shots, X is a matrix of dimensions [m,n], where m is the number of shots in the sample and n, the number of independent variables considered. The intercept term is considered by adding a first column ones-vector, so the dimensions of X becomes [m, n+1]. As MLR is a supervised statistical method, y, which is the dependent variable vector, is also known and is composed by one of the dependent variables described in detail in section 3.2.2: pressure ratio, Detonation, Dual Slope or consumption velocity. Therefore, dimensions of y are [m, 1].

There are two ways to computationally approach this method. The first one consists in using the

MATLAB toolbox. Indeed, MATLAB provides an statistical and machine learning package, which can be used for these kind of studies, although not recommended for complex analysis. However, for MLR, MATLAB offers its own functions, `mnrfit` and `fitlm`, for logistic and linear regression, respectively. Both functions return the regression coefficients θ_i after being provided with matrix X and vector y. The main difference between them is the use of the sigmoid function, as discussed in Section 2.1.

The other way consists in manually implementing the *gradient descent* method. This gradient descent method is the optimization method that both MATLAB functions `mnrfit` and `fitlm` use. In fact, both ways were checked and the same result was obtained. This method aims to minimize the cost function, which represents how different the solution is from the actual result, changing the weights vector θ until reaching convergence. The algorithm includes the following steps:

1. `Weights initialization`

   `Theta = zeros(n+1,1)`

2. `Implement Gradient Descent`

   (a) `Set step parameter` α`:`

   $\alpha = 0,1$

   (b) `Loop until convergence of weights vector` θ

   i. `Set Hyphotesis:`

   $h_\theta(X) = X\theta$ `, if linear regression.`

   $h_\theta(X) = g\left(X\theta\right)$ `, if logistic regression.`

   ii. `Set Cost function:`

   $j(\theta) = \frac{1}{m}\sum_{i=1}^{m}\left[y^{(i)}\log h_\theta\left(x^{(i)}\right) + \left(\left(1-y^{(i)}\right)\right)\log 1 - h_\theta\left(x^{(i)}\right)\right]$

   iii. `Update weights vector` θ`:`

   $\theta_j = \theta_j - \alpha\frac{\partial}{\partial\theta_j}J(\theta)$

   $\theta_j = \theta_j - \alpha\frac{1}{m}\sum_{i=1}^{m}\left(h_\theta\left(x^{(i)}\right) - y^{(i)}\right)\Delta x_j^{(i)}$

   `for j = 1 to n+1.`

The step parameter α represents how big is the variation of the different coefficients θ_i at each iteration. Thus, if this parameter is too high, the gradient descent method may not converge. Conversely, if it is too small, the algorithm may work slowly and, due to the limited number of iterations, it may not lead to convergence. It has been proven that, for normalized features, the value α = 0,1 offers a good compromise regarding computational speed and convergence efficiency [29].

3.3.3 Neural Network

Figure 3.14 represents the structure and dimensions of the neural network created along this project.

As explained before, MLR is applied as many times as the number of units in the hidden and output layers of our neural network, in order to train the algorithm. Once the algorithm has learnt from the shots sample, the returned weights matrices $\Theta^{(1)}$ and $\Theta^{(2)}$ are used to estimate the probabilities of dependent

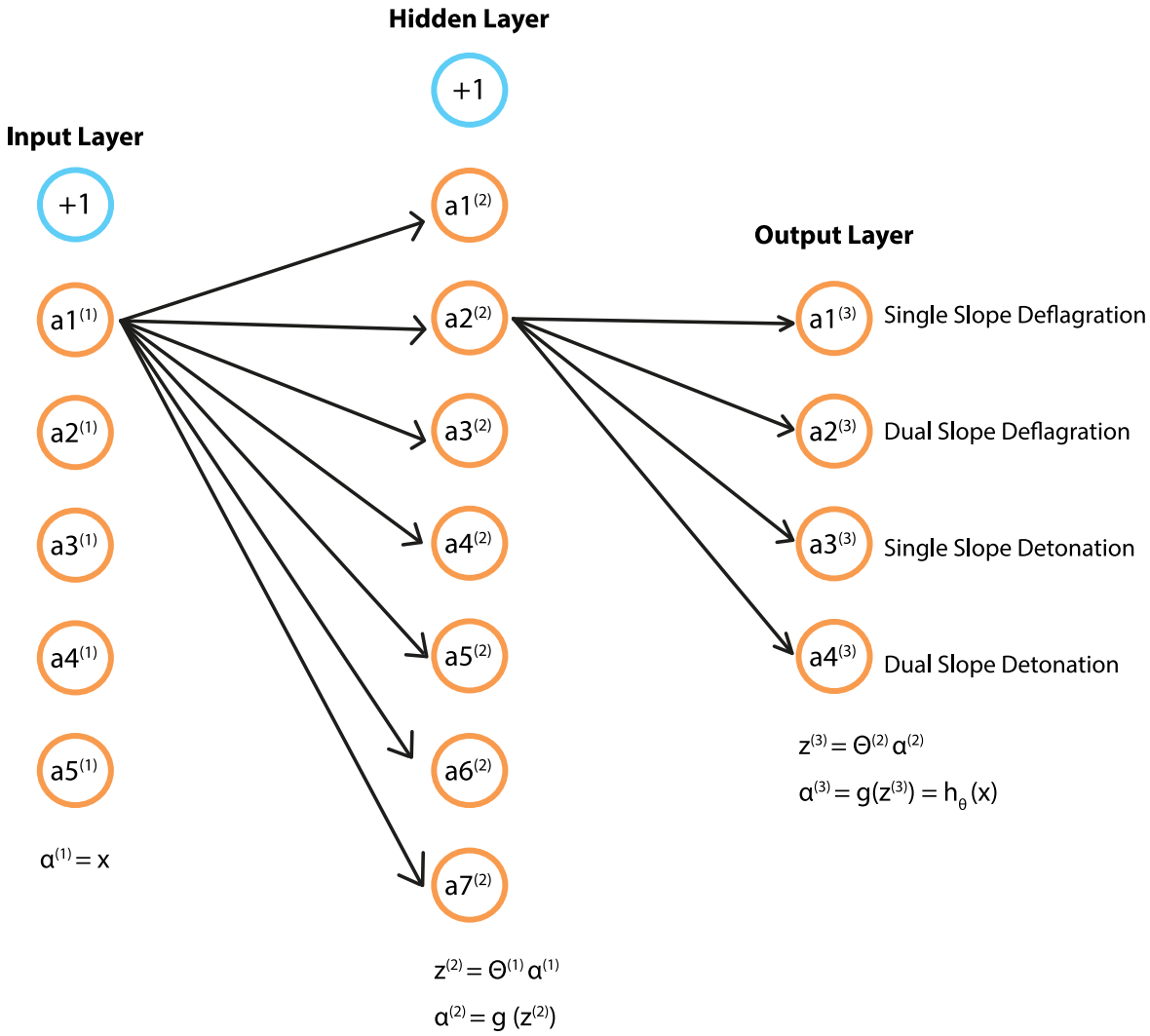

Figure 3.14: Neural network schematics.

variables for which the neural network has been trained. Note that in the neural network, more than one weights/coefficients matrix can be returned; it will depend on the number of layers.

The following sections summarize and analyse the main parts of the neural network.

Structure

- Independent variables vector, X_i. This vector represents the independent variables of the system:

$$X_i = [T_0, p_0, \phi, dil, lens]_i$$

  There are as many of these vectors as the number of shots (i) within the sample, and all of them are concatenated to form the independent variables matrix X. As seen in MLR, a first column composed by ones is added in order to model the intercept term. Therefore, dimensions of X are [m, n+1].

- Dependent variable matrix, y. As stated before, the dependent variable ignition regime is the most important variable in this study, so the neural network will focus on it. Hence, the neural

network will face a multiclass classification problem, and will return the expected regime after certain experimental onset. In order to put the algorithm to work, the discrete dependent variable has to turn into a matrix, so each row represents a shot; and every column, a possible regime. This matrix will be formed by zeros except for those regimes indicated in the dependent variables vector, which will turn into ones. Equation (3.13) represents this transformation:

$$y = \begin{bmatrix} 1 \\ 3 \\ 4 \\ 2 \end{bmatrix} \rightarrow y = \begin{bmatrix} 1 & 0 & 0 & 0 \\ 0 & 0 & 1 & 0 \\ 0 & 0 & 0 & 1 \\ 0 & 1 & 0 & 0 \end{bmatrix} \tag{3.13}$$

Note that this is a result of the multiclass classification nature of the algorithm. Therefore, the other dependent variables, pressure ratio and consumption velocity, must be transformed into discretes variables such as ignition regime, in order to fit this kind of network.

- Hypothesis, h_Θ. The hypothesis vector, which also appeared in MLR, represents the neural network prediction for y. Therefore, it has the same dimension than the dependent variable matrix y, but is composed by real numbers within the interval [0, 1], due to the use of the sigmoid function. As in MLR, the hypothesis represents the product of the matrix X and the coefficients Θ, with intermediate sigmoid transformations.

$$h_\Theta(X) = g\left(\Theta^{(2)}a^{(2)}\right) = g\left(\Theta^{(2)}g\left(\Theta^{(1)}a^{(1)}\right)\right) = g\left(\Theta^{(2)}g\left(\Theta^{(1)}X\right)\right) \tag{3.14}$$

  It represents a probability estimation for each one of the ignition regimes, so a good hypothesis for the prediction of ignition regime 1, single slope deflagration (y = [1 0 0 0]), would be h_Θ = [0,98 0 0 0,002], for instance, which means that the considered experimental onset has 98% probability of returning ignition regime 1, and just 0,2% of returning ignition regime 4 (dual slope detonation). A good hypothesis must be as equal to our results as possible.

- Regularization factor, λ. The regularization factor prevents the weights $\Theta_{ij}^{(l)}$ to grow too large by including a new term in the *cost function*, which is explained in the next item. This helps prevent overfitting, i.e. the problem of the weights matrices $\Theta^{(1)}$ and $\Theta^{(2)}$ matching so perfectly the data sample. This overfitting can lead to an unreal model that could work in a bad way with new train examples. By counterpart, an unappropiate regularization factor can lead to the opposite problem, underfitting. Both situations are represented in Fig. 3.15.

  Figures 3.15a and 3.15b show how results depend on the value of the regularization factor. These pictures represent an hypothetical case of Microchip development, where two different properties are needed to be within a margin around a set value, for instance working temperature and chip size. The algorithm should create a model able to distinguish the valid Microchips (black crosses)

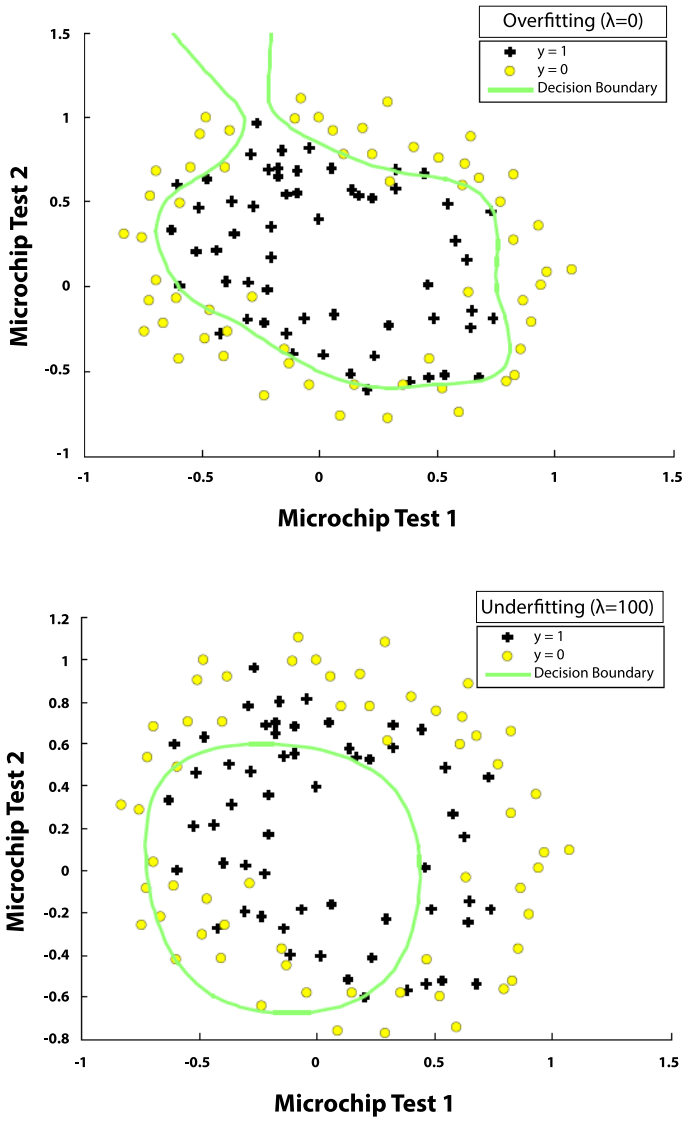

Figure 3.15: Effect of the regularization factor, considering a) $\lambda = 0$ (Overfitting) and b) $\lambda = 100$ (Underfitting).

and Microchips that do not fulfill these requirements (yellow dots). The green line represents the imaginary decision boundary that separates this two-dimensional space into the two possible decisions taken by the algorithm. Therefore, valid Microchips should remain at one side of this decision boundary, whereas rejected Microchips should be at the other side. In Fig. 3.15a, no regularization factor was applied, and that led to overfitting; the decision boundary that separates the predictions of a dichotomous variable does not seem very accurate for high values of the variable Microchip Test 2. On the other hand, for high regularization factors, underfitting arose, leading to an equally erroneous prediction, as seen in Fig. 3.15b.

Regularization factor was not necessary in MLR due to the low number of coefficients and the inherent simplicity of such algorithm. However, it can be easily implemented in MLR models, but results obtained after some testing demonstrated that it is not necessity. Neural networks

have many more weights assigned to independent variables or activation units and, therefore, the implementation of the regularization factor becomes highly recommended.

- Cost function, J. The cost function represents howaccurate are the predictions returned by the current weights matrices $\Theta^{(1)}$ and $\Theta^{(2)}$. The dimensions of these weights depend on the number of hidden units we have and the number of possible outputs, as well as the number of independent variables in the system. Note that the cost function is really similar to the one used in MLR, but this one includes a second term to model the regularization factor λ.

  The cost function $J(\Theta)$ is given by Eq. (3.15),

$$J(\Theta) = -\frac{1}{m}\left[\sum_{i=0}^{m}\sum_{k=1}^{K} y_k^{(i)} \log\left(\left(h_\Theta\left(x^{(i)}\right)\right)_k\right) + \left(1 - y_k^{(i)}\right)\log\left(\left(1 - h_\Theta\left(x^{(i)}\right)\right)_k\right)\right] + \frac{\lambda}{2m}\sum_{l=1}^{L-1}\sum_{i=1}^{s_l}\sum_{j=1}^{s_{l+1}}\left(\Theta_{ji}^{(l)}\right)^2 \tag{3.15}$$

  where K represents the number of possible output units, i.e. the possible classes that our multi-class classification neural network must fit. In the study of the dependent variable ignition regime, four possible regimes are eligibles, so K = 4. Lastly, L represents the number of layers and s_l, the number of units in each layer L.

  The goal of the algorithm is to reduce this function as much as possible, variating the weights matrices $\Theta^{(1)}$ and $\Theta^{(2)}$.

- Gradient of the cost function. This variable represents the gradient of the cost function respect to every $\Theta_{ij}^{(l)}$.

$$\frac{\partial}{\partial \Theta_{ij}^{(l)}} J(\Theta)$$

  For most of optimization tools, this variable must be provided in order to drive the algorithm towards the right direction during iterations. It is calculated by the *backpropagation algorithm*.

- Backpropagation algorithm. The backpropagation algorithm is the main method chosen to build the neural network. At each iteration, this algorithm calculates the gradient of the cost function with respect to every different $\Theta_{ij}^{(l)}$. This algorithm includes the following steps:

  1. `Training set`

     $\left(x^{(i)}, y^{(i)}\right), ..., \left(x^{(m)}, y^{(m)}\right)$

  2. `Set accumulated error (used to compute the gradient of the cost function)`

     $\Delta_{ij}^{(l)} = 0$

     `for all i, j and l.`

  3. `Loop For i = 1 to m`

     (a) `Set`

     $a^{(1)} = x^{(i)}$

     (b) `Forward propagation to compute` $a^{(l)}$ `for l = 2, 3, ..., L`

(c) Using $y^{(i)}$, compute $\delta^{(L)} = a^{(L)} - y^{(i)}$

(d) Compute $\delta^{(L-1)}, \delta^{(L-2)}, ..., \delta^{(2)}$

i. $\delta^{(L-1)} = \Theta^{(L-1)}\delta^{(L)} g'\left(z^{(L-1)}\right)$

ii. $g'(x) \equiv$ gradient of the sigmoid function

iii. $g'\left(z^{(l)}\right) = a^{(l)}\left(1 - a^{(l)}\right)$

(e) $\Delta_{ij}^{(l)} := \Delta_{ij}^{(l)} + a_j^{(l)}\delta_i^{(l+1)}$

4. $D_{ij}^{(l)} := \frac{1}{m}\Delta_{ij}^{(l)} + \lambda\Theta_{ij}^{(l)}$ if j $\neq 0$

5. $D_{ij}^{(l)} := \frac{1}{m}\Delta_{ij}^{(l)}$ if j $= 0$

6. $\frac{\partial}{\partial\Theta_{ij}^{(l)}} J(\Theta) = D_{ij}^{(l)}$

This algorithm updates the weights matrices $\Theta^{(1)}$ and $\Theta^{(2)}$ just as gradient descent algorithm does in MLR. However, the increased complexity of the neural network makes this algorithm unable to accept zero matrices as initial weights matrices, like MLR does. In this case, a symmetry problem occurs, so every activation unit in the neural network would update to the same value. Therefore, a non symmetrical initialization of matrices $\Theta^{(1)}$ and $\Theta^{(2)}$ is needed.

Sample division

In order to experiment, upgrade and improve the neural network, the sample of shots was divided in three sets: training set, cross validation set and testing set.

- Training set. Represents 60% of the whole sample, and is used to train the neural network, to update the $\Theta_{ij}^{(l)}$.
- Cross validation set. Composed by a 20% of the shots. It is used to determine the optimal regularization factor, since it must be determined with a set of shots that does not belong to the sample that trains the algorithm; otherwise, the results may be tricked.
- Testing set. Formed by the rest of the sample, 20%. Checks the behavior of the neural network with completely unknown examples. Once the algorithm has stopped running, and the matrices $\Theta^{(1)}$ and $\Theta^{(2)}$ are returned, it is good to see how accurate are the predictions of new shots.

These sets are randomly generated from the fifty shots of the sample during each test, so the results may differ from one run to another. In order to deal with the uncertainty, the number of iterations must be high enough. Nevertheless, due to the complex domain, this solution will solve the issue just partially.

Accuracy

There are basically three parameters that can be varied in order to reach the maximum level of neural network accuracy. These parameters are the regularization factor, the number of iterations and number of hidden units. Besides, the weights matrices must be randomly initialized to avoid a symmetry problems.

The symmetry problem appears when iniatializing all $\Theta_{ij}^{(l)}$ to the same value. While the MLR method worked perfectly with zeros as initial θ_i, the backpropagation algorithm does not allow such decision. Instead, all nodes would update to the same value iteratively, and hence the neural network algorithm would not advance. In order to avoid this problem, every $\Theta_{ij}^{(l)}$ is set to random number around zero, within the interval [-ε_{init}, ε_{init}], at the beginning of each run. Here, ε_{init} is an arbitrary constant used to set the random initialization interval to a reasonable value. An effective strategy is to base ε_{init} on the number of units in the network. A proven good choice is given by Eq. (3.16),

$$\varepsilon_{init} = \frac{\sqrt{6}}{\sqrt{L_{in} + L_{out}}} \tag{3.16}$$

where $L_{in} = s_l$ and $L_{out} = s_{l+1}$ are the number of units in the adjacent layers to $\Theta^{(l)}$.

Once the weights have been initialized, the regularization factor is set. The cost function is computed for different values of regularization factor. Figure 3.16 shows the error as a function of the regularization factor used in the algorithm.

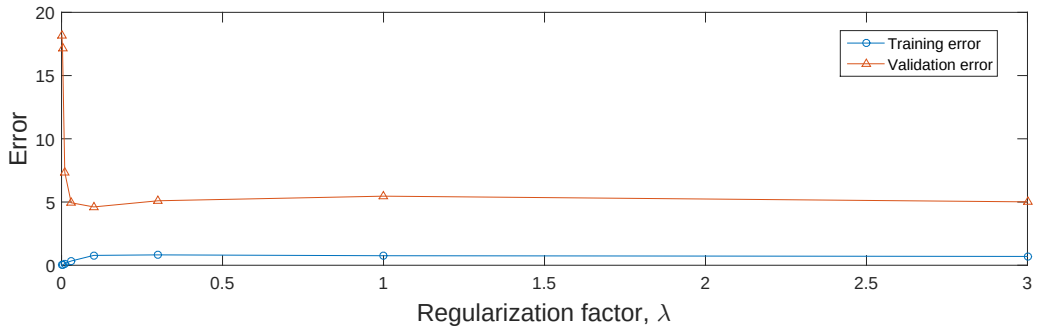

Figure 3.16: Errors vs. regularization factor.

In Fig. 3.16, the errors represent the cost function analysed in the training set and in the cross validation set. To compute these errors, no regularization factor was used, except for calculating the matrices of weights $\Theta^{(1)}$ and $\Theta^{(2)}$. Therefore, the cost function depends just on these weights matrices. The results show that the validation error has a minimum around λ = 0,1. It has been proven as well that this error stabilizes for regularization factors of above 3 ($\lambda > 3$). Moreover, the training error is lower than the validation error because the network has learned from the training set and, as expected, it tends to fit that set.

The random initialization of the weights matrices makes the optimum λ different from one run to the next one. Consequently, a new function is implemented in the neural network. This function analyses different regularization factors and chooses the one that minimizes the validation error. Once the regularization factor is chosen, the training and validation set will merge, allowing the network to learn from a larger database, increasing its performance.

It is also interesting to analyse the evolution of the cost function J as a function of the number of iterations performed. Figure 3.17 shows that the cost function decreases with the increase of the

number of iterations.

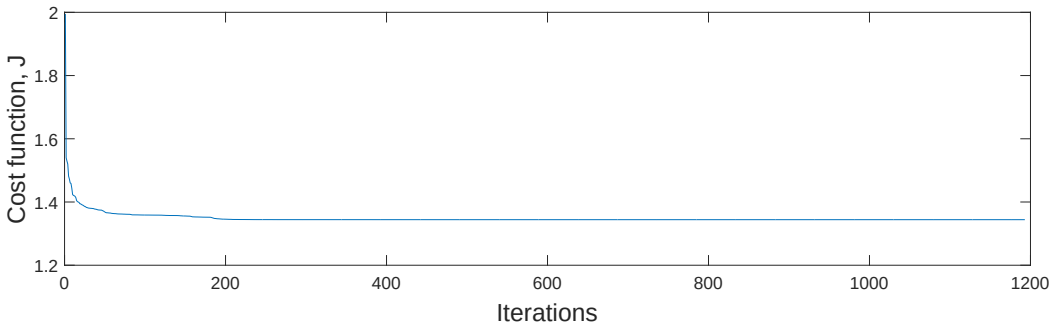

Figure 3.17: Cost function vs. number of iterations.

This result is intuitive since the algorithm reduces the cost function step by step, inducing slight changes in the weights map. In order to fulfill our goals, the neural network will work with a number of iterations as high as necessary. Therefore, part of its performance consists in stopping running if the cost fuction does not variate along several iterations, i.e. if the algorithm converges.

Focusing now on the number of units in the hidden layer, which represents different relations between our independent variables, the cost function has been plotted for different number of hidden units, as seen in Fig. 3.18.

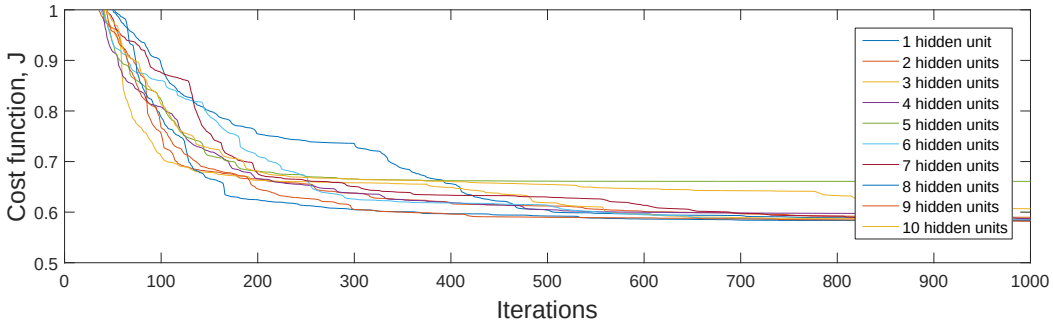

Figure 3.18: Cost function vs. number of units in the second layer.

The curves shown in Fig. 3.18 represent the evolution of the cost function as a function of the number of units in the second layer. Most of these curves converge to the same value, yet the normalization of the variables and the implementation of the regularization factor makes this value very reduced. The difference between performances regarding number of hidden units relies in small decimal digits. However, some of of the experiments shown in Fig. 3.18 offer good results with a lower number of iterations. After some testing, it was found that the optimal number lies between six and eight hidden units. Onwards, this interval will be considered.

3.3.4 PCA

The Principal Component Analysis algorithm is very useful tool, used for reducing the complexity of problems. ESTHER combustion is considered a five-dimensional problem; each independent variable represents one dimension. Thus, thanks to PCA method these dimensions will be reduced to two, and hence they will be plotted in a graph. This performance is complemented by the K-means algorithm, which is capable of forming clusters of data. These clusters classify the shots by their experimental onset, regardless the outcome (ignition regime, pressure ratio, consumption velocity). The goal is to find a correlation between these clusters and the ignition regimes obtained in ESTHER's shock-tube.

This K-means algorithm works under a very simple principle. First, it randomly selects a number of shots equal to the intended number of clusters. These shots serve as starting points for the clusters centroids, i.e. the "center" of the cluster. In our case, four clusters will be created, one per possible ignition regime. Then, the algorithm will assign iteratively shots to the closest centroid and move those centroids within the five-dimensional space in order to fit better the sample, i.e. reduce the total distance from each point/shot to their assigned centroid. The algorithm includes the following steps:

1. `Centroids randomly initialized`

   $\mu_k := x^{(i)}$

2. `Loop For iter = 1 to iterations`

   (a) `Cluster assignment`

   $c^{(i)} := j$ `that minimizes` $||x^{(i)} - \mu_j||^2$,

   `for i = 1 to m and j = 1, 2, 3 or 4.`

   (b) `Centroid means`

   $\mu_k := \frac{1}{|C_k|} \sum_{i \in C_k} x^{(i)}$,

   `where` C_k `is the set of shots assigned to centroid k.`

The performance of this algorithm can be seen in Fig. 3.19, where a simpler 2-D problem undergoes this method.

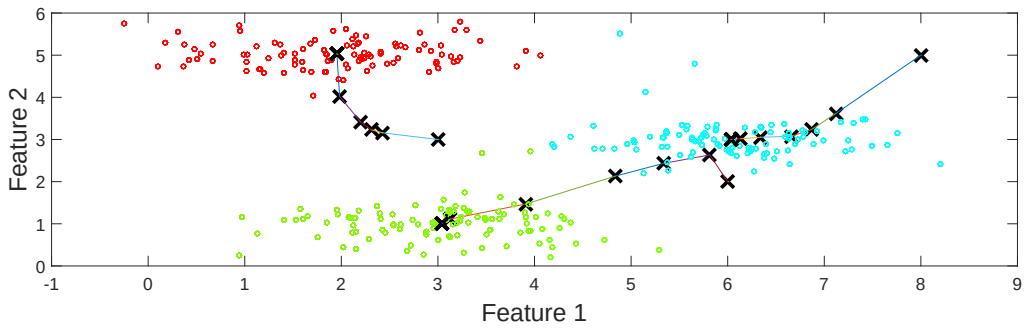

Figure 3.19: K-means algorithm clustering process.

Once this algorithm clustered the sample of shots, regarding the independent variables but with no knowledge about the ignition regime triggered by those features, PCA is used to reduce the dimensions of the problem so the clusters are observable in this manuscript.

The PCA dimension reduction process consists in a series of projections into lower dimensional space. The dimension to be reduced is the dimension that presents less deviance with respect to its mean value. After this projection, the problem will lose the dimension where the data were projected. The projection is achieved by obtaining the eigenvectors of the features matrix, which is composed by all the shots in the database, so it has dimension [m,n]. Notice that this matrix is the same independent variables matrix X used in MLR and Neural Network, but without the first ones-column used to model the intercept term. This operation is repeated as many times as necessary until the desired number of dimensinos is reached; two in our case. The algorithm includes the following steps:

1. `Features normalization`
2. `Principal components`
   (a) `Compute the covariance matrix`
   $\Sigma = \frac{1}{m} X^T X$
   (b) `Compute the principal components, eigenvectors`
   `[U, S, V] = svd(`Σ`), so that` Σ `= U*S*V`^{T}`,`
   `where svd = singular value decomposition and U contains the principal components.`
3. `Data projection`
   $Z(i,k) = X(i,:)U(:,k)$
   `for i = 1 to m and k = 1 to final dimensions number. Z = projected data matrix.`

Figure 3.20 shows an hypothetical example of the PCA performance, which does not use any of the variables involved in ESTHER combustion.

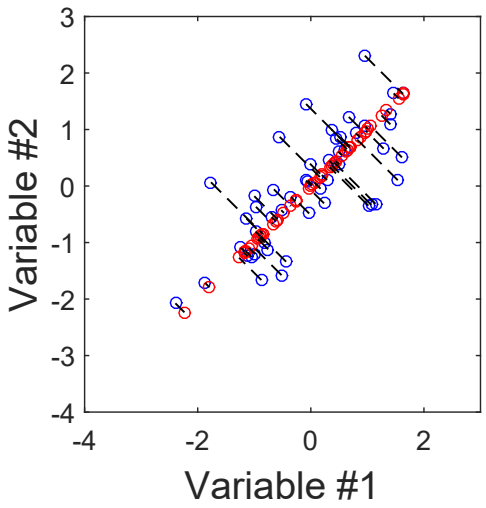

Figure 3.20: PCA dimension reduction.

The blue dots represents the original sample of examples whereas the red dots are the projected examples. It can be seen that all the examples has been projected into a line, which is a one-dimensional space, following the direction of the features principal component, given by the eigenvector of the sample.

Chapter 4

Results

The statistical analysis performed in this chapter includes the study of the regression equations returned by MLR algorithm, the graphs generated by the trained neural network and the study of the clusters returned by the PCA algorithm.

As stated in Section 3.3.1, the regressions returned by MLR, as well as the results provided by the neural network use normalized data, so the magnitude order of the variables' variation is the same. Hence, the coefficients θ_i provide qualitative information about the influence of the independent variables in the probability of a given event. The normalization of the variables is given by Eq. (4.1), which summarizes the process explained in Section 3.3.1,

$$x := \frac{x - \mu_i}{s_i} \tag{4.1}$$

where μ_i is the mean value of the variable i and s_i is the considered range of this variable i ($s_i = x_{i_{max}} - x_{i_{min}}$). Table 4.1 shows the μ_i and s_i values of each independent variable.

Variable	μ_i		s_i	
Initial temperature, T_0	19,9	ºC	14,0	ºC
Initial gas pressure,p_0	38,2	bar	88,0	bar
Equivalence ratio, ϕ	0,95		1,00	
Helium dilution, dil	0,72		0,20	
Use of lens, $lens$	0,44		1	

Table 4.1: Normalization parameters.

In Table 4.1, it is unrighteous to say that the average ignition source is $lens$ = 0,44. A dichotomous variable, such as lens, has no concept of average. However, laser without lens ($lens$ = 0), which has a normalized value of -0,44, is the most common ignition source within the sample. Henceforth, it is referred as the average experimental onset the onset that uses the normalized mean value of each independent variable, considering laser without lens as ignition source (Average onset: T_0 = 0, p_0 = 0, ϕ = 0, dil = 0, $lens$ = -0,44). This average onset is used to test the neural network performance along this

section.

The analysis with MLR presented in this chapter provides the *p-values* of each independent variable. These p-values help determine the significance of the results in the *Null hypothesis* tests (Null hypothesis: the independent variable has no correlation with the dependent variable). Therefore, the p-values are assigned to each independent variable (T_0, p_0, ϕ, dil, $lens$) and to the intercept term. A small p-value (typically $\leq 0,05$) indicates strong evidence against the null hypothesis, which means that the independent variable is statistically correlated to the dependent variable. Conversely, a large p-value ($> 0,05$) indicates weak evidence against the null hypothesis, so the latter applies, which means that the independent variable does not correlate with the dependent variable.

Considering the statistical analysis with the method Neural Networks, it is important to remark that all the available shots have trained the algorithm. Therefore, once the regularization factor has been chosen, all the three sets explained in Section 3.3.3 merge and the neural network is trained using the whole sample of shots in order to build the most accurate model. This performance provides the best weights matrices $\Theta^{(1)}$ and $\Theta^{(2)}$, necessary to understand the physics underlying the ESTHER combustion. Moreover, the Neural Networks algorithm must run several times in order to check the influence of the random initialization of the matrices $\Theta^{(1)}$ and $\Theta^{(2)}$, as discussed in Chapter 3.

The accuracy of the statistical methods is also discussed in this section. For dichotomous/discrete variables, the accuracy is defined by the number of shots correctly predicted over the total number of shots. Yet, for non discrete variables such as pressure ratio and consumption velocity, accuracy is designated by the mean relative error.

The results obtained from the supervised statistical methods (MLR and Neural Networks) are organized regarding the three dependent variables: ignition regime, pressure ratio and consumption velocity. The results obtained with PCA method are presented separately, as it does not directly relate to any dependent variable due to the algorithm's unsupervised nature.

4.1 Ignition Regime results

4.1.1 MLR

In order to predict the ignition regime variable, MLR offers two different regressions, one for each dichotomous variable: Detonation and Dual Slope. The combination of these two regressions will return the respective probability of each regime to occur.

Detonation

The results of the analysis of Detonation with MLR are shown in Table 4.2:

As seen in Table 4.2, the initial temperature (p-value = 0,84) and initial gas pressure (p-value = 0,93) are not correlated to the event of a detonation. Equivalence ratio is slightly more correlated, yet its p-value is still above the 0,05 threshold to validate the strong correlation. Helium dilution (p-value = 0,02)

Variable	θ_i	p-values
Intercept term	-1,88	10^{-5}
Initial temperature, T_0	-0,31	0,84
Initial gas pressure, p_0	-0,16	0,93
Equivalence ratio, ϕ	-1,92	0,30
Helium dilution , dil	-4,99	0,05
Use of lens, $lens$	0,79	0,49
Accuracy	88,5%	

Table 4.2: MLR coefficients for dependent variables Detonation.

is the most important value to statistically predict whether detonation or deflagration occur. Indeed, values of helium dilution below the average (dil = 0,72) lead the regression likely to predict detonation, as can be inferred from the assigned coefficient (θ_i = -4,99). Lens are not considered really relevant in this regression, as given by the variable's p-value, but neural network results will deny this hypothesis showing that this variable does have importance. Still, this regression correctly predicted the detonation event for 88,5% of the shots, which is actually a solid value. The accuracy obtained is related with the distribution of the dependent variable in the shots sample. As can be seen in Fig. 3.10, deflagration is considerably more common than detonation. Therefore, MLR tends to predict this regime for being statistically more probable to occur. The analysis of the predictions shows that all the mispredicted shots are indeed detonations predicted as deflagrations.

The regression equation for the dependent variable Detonation, which uses the coefficients θ_i seen in Table 4.2, is given by:

$$P(Detonation) = g\left(-1,88 - 0,31T_0 - 0,16p_0 - 1,92\phi - 4,99dil + 0,79lens\right) \tag{4.2}$$

Equation 4.2 shows how the independent variables correlate with the probability of a detonation event. The intercept term (θ_i = -1,88) shows that the average probability of detonation, that using the average experimental onset, is 9,7%. If the optical configuration is changed to lens ($lens$ = 1), the probability of detonation increases to 19,2%. Moreover, the estimated coefficients indicates that an unitary increase in the initial temperature, while the rest of variables remain constant, produces a mean decrease of 0,2% in the probability of detonation event (ΔT_0 = 1°C $\rightarrow$ ΔP(Detonation) = -0,2%). Likewise, unitary increases of initial gas pressure and mixture equivalence ratio induce decreases of similar magnitude order in the probability of detonation to occur (Δp_0 = 1 bar $\rightarrow$ ΔP(Detonation) = -0,02%; $\Delta\phi$ = 0,1 $\rightarrow$ ΔP(Detonation) = -1,2%). The coefficient assigned to dil, θ_i = -4,99, is the largest within the estimated coefficients, yet the variations of helium dilution are usually small with respect to the mean value (dil = 0,72). Therefore, an increase of 0,01 in the dilution factor means that the prediction of detonation decreases 3,9% (Δdil = 0,01 $\rightarrow$ ΔP(Detonation) = -3,9%). It is concluded that helium dilution is is the independent variable statistically more correlated with detonation predictions.

Dual slope

Here we want to identify the independent variables correlated to the dual slope phenomena. Dual Slope variable refers to the inflection in the pressure-time curve, which was said to be related with tulip flames. Table 4.3 shows the coefficients obtained after the analysis with MLR.

Variable	θ_i	p-values
Intercept term	-3,10	10^{-3}
Initial temperature, T_0	-6,90	0,02
Initial gas pressure, p_0	-2,60	0,37
Equivalence ratio, ϕ	-0,18	0,96
Helium dilution , dil	9,40	0,18
Use of lens, $lens$	-3,90	0,02
Accuracy	92,3%	

Table 4.3: MLR coefficients for dependent variable Dual Slope.

The p-values shown in Table 4.3 reveal that the variables more correlated to the dual slope event are the initial temperature (p-value = 0,02) and the use of lens (p-value = 0,02). Dual slope formation seems to be independent of the mixture equivalence ratio, but slightly dependent on the initial gas pressure. Considering the helium dilution, the p-value is above the 0,05 threshold, but its assigned coefficient (θ_i = 9,40) is large enough to induce important changes in the dual slope predictions. In this case, high dilutions factors trigger the dual slope phenomena. However, it is important to note that dilution factor is a variable with little variation regarding its average value (see Fig. 3.5). As menctioned, lens is an important variable in Dual Slope regression, being that if the laser is shot unfocalized ($lens$ = 0), probabilities of having dual slopes increase. The model for this variable fitted the sample in a better way than Detonation regression, returning an accuracy of 92,3%, which is also a really solid value, even when it is also affected by the distribution of the dependent variable within the shots sample.

The regression equation for the dependent variable Dual Slope is given by Eq. (4.3).

$$P(DualSlope) = g\left(-3,10 - 6,90T_0 - 2,60p_0 - 0,18\phi + 9,40dil - 3,90lens\right) \tag{4.3}$$

The negative intercept term (θ_i = -3,10) shows that, regardless the ignition source used (without lens or with lens), the probability of dual slope is desfavorable for both cases, yet higher when lens are not used ($lens$ = 0 $\rightarrow$ P(Dual Slope) = 20,2%; $lens$ = 1 $\rightarrow$ P(Dual Slope) = 0,5%). Coefficients assigned to initial temperature (θ_i = -6,90), initial gas pressure (θ_i = -2,60) and equivalence ratio (θ_i = -0,18) are all negative. This means that an unitary increase in these independent variables, while the rest of variables remain constant, provokes a decrease in the probability of dual slope. In fact, the mean decrease in dual slope probability is 5,8% for initial temperature (ΔT_0 = 1ºC $\rightarrow$ ΔP(Dual Slope) = -5,8%), 0,4% for initial gas pressure (Δp_0 = 1 bar $\rightarrow$ ΔP(Dual Slope) = -0,4%) and 0,3% for equivalence ratio ($\Delta\phi$ = 0,1 $\rightarrow$ ΔP(Dual Slope) = -0,3%). However, high values of helium dilution provokes increases in the dual slope

probability. The estimated coefficient (θ_i = 9,40) means an increase of 3,2% per 0,01 dilution factor (Δdil = 0,01 $\rightarrow$ ΔP(Dual Slope) = 3,2%). Estimated coefficients θ_i shown in Eq. (4.3) have higher absolute value than the respective coefficients observed in the analysis of Detonation (Eq. 4.2), which means that dual slope event is more influenced by the experimental onset than detonation event, mainly correlated with the dilution factor.

The results in this section show that MLR provides a good approach to the understanding of the physics underlying ESTHER combustion. Still, the linear nature of the correlations with MLR provokes some flaws that can be solved using a more sophisticated algorithm, such as Neural Networks.

4.1.2 Neural Network

In order to successfully predict the dependent variable Ignition Regime, the neural network was built to front a multiclass classification problem. Therefore, it returns the probability of each regime to happen. The particular pair of matrices $\Theta^{(1)}$ and $\Theta^{(2)}$ used in this section can be found in Appendix B.

The study of the influence of the of independent variables in the ignition regime prediction proceeds by variating one of the independent variables from the average experimental onset, which was introduced at the beginning of this chapter. The first variable to be tested is the use of lens. Later, the rest of independent variables are also analysed.

- **Impact of the use of lens, $lens$.** Table 4.4 shows the difference in the probability prediction with respect to the ignition source given by the Neural Network analysis.

Ignition regime	Probability	
	Without lens	With lens
Single slope deflagration	35,7%	4,4%
Dual slope deflagration	14,0%	24,8%
Single slope detonation	5,2%	76,2%
Dual slope detonation	6,2%	1,0%

Table 4.4: Ignition regime probability distribution regarding the ignition source.

Probabilities in table 4.4 show that, for the average onset tested with and without lens, a substantial difference exists. Without lens, the neural network offers a poor probability distribution. It predicts single slope deflagration as the event likely to occur, but the probability returned, 36%, is considerably low compared with the results commonly returned. When lens are engaged, the neural network predicts single slope detonation with a probability of 76,2%. Therefore, the table confirms the intuitive conclusion obtained from the preliminary analysis: when the laser is focused on one point, sharper temperature gradients cause higher peaks of energy within the gas mixture, allowing more energetic phenomena, such as detonation. However, $lens$ seems not to have a strong influence in the predictions of dual slopes, as shown by the analysis with MLR. This conclusion is

only valid for the considered average onset.

Figures 4.1-4.4 show the probability distribution of each ignition regime (Single slope deflagration, Dual slope deflagration, Single slope detonation and Dual slope detonation) for the range of values of the independent variables (Initial temperature, initial gas pressure, equivalence ratio and helium dilution) and both ignition sources (without lens and with lens).

- **Impact of the initial temperature, T_0.**

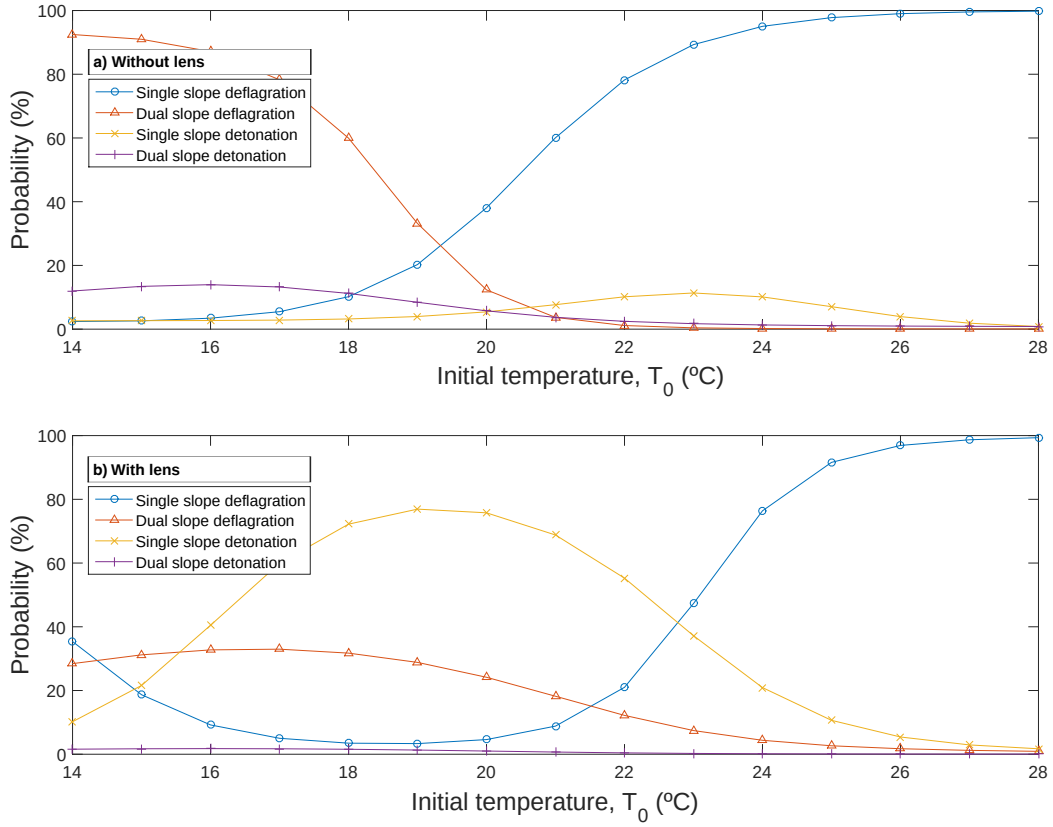

Figure 4.1: Ignition regime probability distribution regarding T_0, conditioned by (a) without lens and (b) lens.

Figure 4.1a shows that, without lens, for low initial gas temperatures (from 14 to 19 ºC) the most probable ignition regime is the dual slope deflagration (about 90% probability), whereas for high initial gas temperatures (from 21 to 28 ºC) the single slope deflagration is the most probable ignition regime (monotonic rise from 50% up to 100% within this temperature range). Moreover, within this range of inital gas temperature, Fig. 4.1a shows very low probabilities for a detonation event if the shot is performed without lens. On the other hand, if the shot is performed with lens (Fig. 4.1b), for initial gas temperature around 19 ºC, detonation is the most likely ignition regime with a probability around 80%. These results agree well with those obtained with MLR method only for the case without lens. The discrepancy of MLR and Neural Network results observed for the case of Fig. 4.1b is explained by the quadratic probability distribution of the detonation regime with the

gas temperature, which can not be captured by the MLR method (linear dependency).

- **Impact of the initial gas pressure, p_0.**

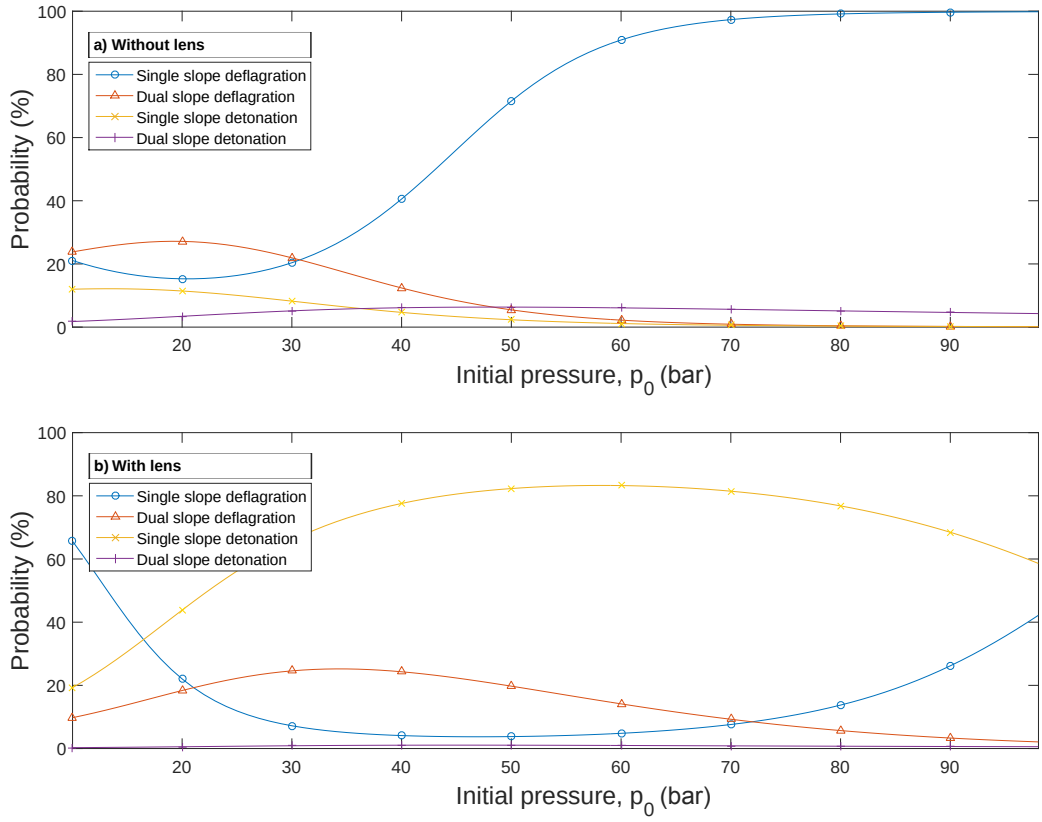

Figure 4.2: Ignition regime probability distribution regarding p_0, conditioned by (a) without lens and (b) lens.

Figure 4.2a shows a monotonic increase of the single slope deflagration probability from 30% to 100% within the interval of 35 and 100 bar gas filling pressures. For p_0 below 35 bar, with a probability of 35%, the ignition regime most likely to occur is dual slope deflagration. However, the statistical analysis is not conclusive for these low values of the gas filling pressures without lens. Nevertheless, a more conclusive statistical result can be observed, in Fig. 4.2b, when the shot is performed with lens. The results show that for a wide range of gas filling pressures (from 30 up to 100 bar), the ignition regime is likely to be a single slope detonation, with a probability of around 80%. These results show that, from a statistical standpoint, for any gas pressure higher than 30 bar the ignition regime of an average shot with lens will be, with 80% probability, a single slope detonation. Which means that, to change the ignition regime, is more relevant to change the optical system configuration (with or without lens) than varying the gas filling pressure. Nevertheless this conclusion is only valid if the independent variables are those of the average experimental onset, given in the introduction of the present chapter.

- **Impact of the equivalence ratio, ϕ.**

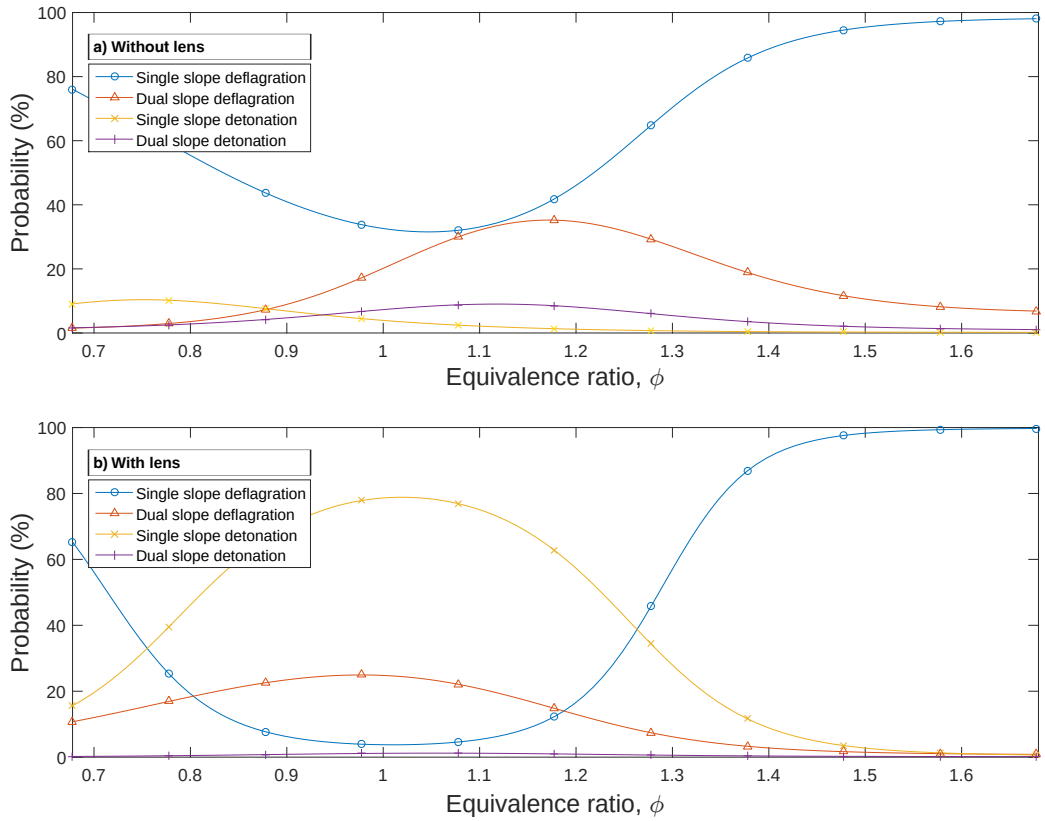

Figure 4.3: Ignition regime probability distribution regarding ϕ, conditioned by (a) without lens and (b) lens.

The results shown in Figs. 4.3a and 4.3b are very expressive. In Fig. 4.3a the statistics show that, if the shot is performed without lens, for all the range of ϕ, the most probable ignition regime is the single slope deflagration. Yet, the single slope deflagration probability distribution with ϕ is not monotonic and reaches a minimum of 40% when the dual slope deflagration probability distribution reaches a peak, for values of ϕ in the range of 1 and 1,3. For equivalence ratios from 1,3 up to 1,7, the probability of single slope deflagration rises near 100%. The results show that detonation has a probability of less than 10% for all the range of ϕ values. These results completely change when the shot is performed with lens, as shown in Fig. 4.3b. In fact, there is a high probability of single slope detonation for values of ϕ near the stoichiometric value (ϕ = 1); in the vicinity of ϕ = 1 the probability of detonation is about 80%. Moreover, the single slope deflagration regime is now shifted towards higher values of ϕ whereas near ϕ = 1 the probability of this regime is less than 5%. It is also interesting to note the quadratic evolution of the single slope detonation probability curve around the stoichiometric value. In fact, this result is explained by the physics of the problem. For mixtures with equivalence ratio ϕ around 1 the transfer of chemical energy into heat is more efficient and therefore the gas temperature increase is higher than that obtained for values of ϕ outside the vicinity of the value one. When the mixture is poor (excess of air/O_2, $\phi << 1$) or rich (excess of fuel, $\phi >> 1$) part of the chemical energy released during the combustion will be

absorbed by the excess of air/O_2 or fuel/H_2 molecules and will be more difficult to trigger the mixture ignition. As observed in Fig. 4.3a and more enhanced in Fig. 4.3b, close to ϕ = 1 the ignition process is more efficient and faster, which may lead to a detonation regime. This also explains the differences observed for the case with lens and without lens. Without lens, the laser energy is deposited inside a volume larger than that when lens are used. Therefore, the energy density in the case of Fig. 4.3a is lower than that in the case of Fig. 4.3b, explaining the higher detonation probability in this last case. The equivalence ratio enhances the energy density differences at the vicinity of ϕ = 1. This quadratic dependency could not have been captured by the linear regression used in the MLR method, although from a physical standpoint it should be modelled.

- **Impact of the helium dilution factor, dil.**

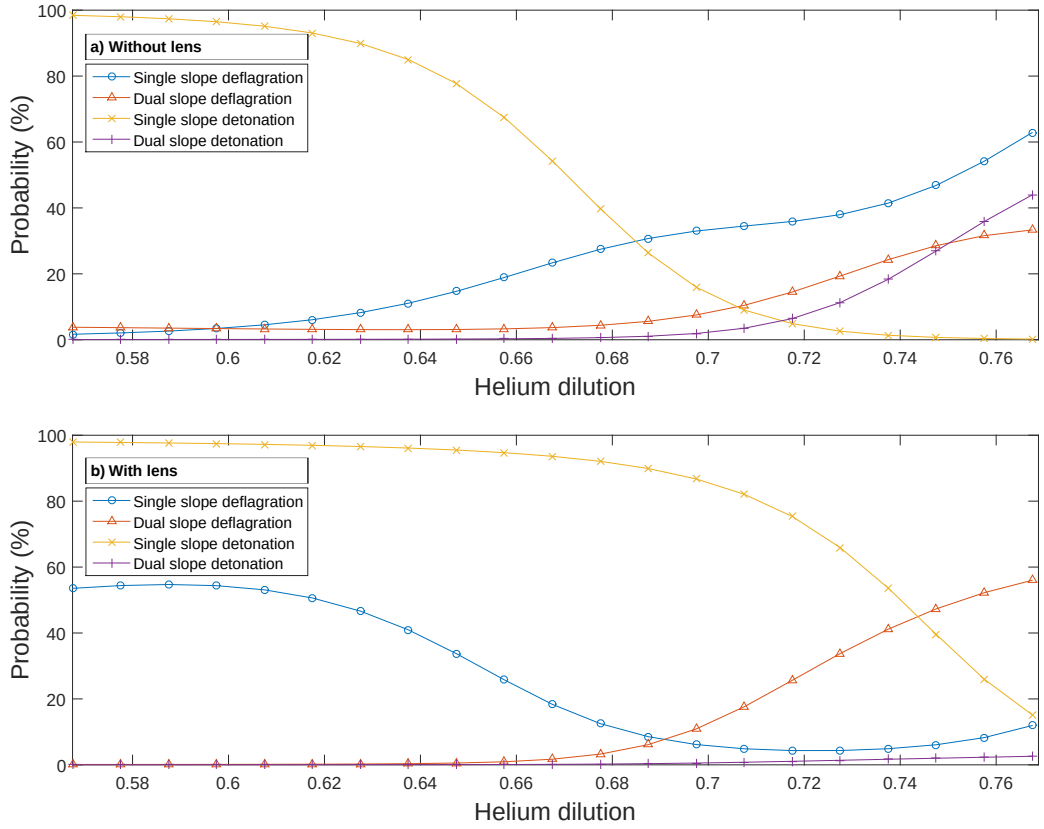

Figure 4.4: Ignition regime probability distribution regarding dil, conditioned by (a) without lens and (b) lens.

Figures 4.4 shows a probability distribution considerably different of those shown in Figs. 4.1, 4.2 and 4.3. Figure 4.4a shows a monotonic decrease of the single slope detonation probability from near 100% to 30% in the range of dilution factors within the interval of 0,57 and 0,69. For higher dilutions values (from 0,69 up to 0,77), the ignition regime most likely to occur when lens are not used is single slope detonation. Moreover, it can be appreciated in Fig. 4.4a that both regimes involving dual slope (dual slope deflagration and dual slope detonation) present an increase for dilution factors above 0,72. Dual slope detonation is a rare ignition regime that lacks information,

since only two shot in the sample returned it. However, a monotonic rise in the dual slope detonation probability, from near 0% up to 45%, is observed for high dilution values ($dil >$ 0,72). From a statistical standpoint, this is a reflection of the experimental onset that triggered dual slope detonation (shot #149, dil = 0,74; and shot #170, dil = 0,72). On the other hand, Fig. 4.4b shows the probability distribution if lens are used to perform the shot. This optical configuration enhances the results observed in the case without lens. Single slope detonation probability is enhanced for the range of dil considered. From dil = 0,68 up to dil = 0,77, single slope detonation probability monotonically decreases from 95% to 15%. Conversely, dual slope deflagration probability presents a monotonic increase for dilutions from 0,68 up to 0,77, from 0% up to 60%. This result is similar to that observed in Fig. 4.4a, yet enhanced by the optical configuration. In fact, from dilutions near 0,74, dual slope deflagration is the regime most likely to be predicted. Moreover, the response of dual slope detonation to the independent variable dil given by Fig. 4.1a is not observed in the case with lens, keeping a probability near 0% for the range of dil considered. The results completely agree with those seen in the MLR analysis, so it can be concluded that low values of helium dilution ($dil <$ 0,70) does not provide the heat absorption necessary to avoid detonations of the mixture.

The final ignition regime prediction is a combination of the unitary influences of the independent variables, given by the graphs shown in this section, so a physical model for the ESTHER combustion can be inferred from these results. These graphs have been used for a first testing, with satisfactory results.

The neural network predicted the dependent variable Ignition regime with 88% of accuracy, which means that only four shots were mispredicted. Considering that two of them are the two shots that returned dual slope detonation (regime that lacks information), it can be concluded that Neural Networks method offers a robust tool to know the presumed ignition regime of certain experimental onset before performing the shot.

The independent variables influence in the ignition regime of the combustion is clear, and an empirical numerical model, based on the statisticall analysis of ESTHER shock-tube combustions, has been created with the regressions shown in Tables 4.2 and 4.3, and with the trained neural network.

4.2 Pressure ratio results

4.2.1 MLR

Pressure ratio is a continuous variable and hence it is not a phenomenon that can happen or not. Multivariate Linear Regression is used to predict the presumed pressure ratio returned by certain onset. This pressure ratio is therefore a non normalized discrete value.

The regression values returned by the Multivariate Linear Regression analysis is given by Table 4.5.

The p-values in Table 4.5 show that initial temperature (p-value = 0,74) and use of lens (p-value = 0,34) are poorly correlated with pressure ratio. Moreover, initial gas pressure (p-value = 0,14) and mix-

	Pressure ratio coefficients	
Variable	θ_i	p-values
Intercept term	7,01	0,00
Initial temperature, T_0	0,20	0,74
Initial gas pressure, p_0	-1,21	0,14
Equivalence ratio, ϕ	-1,37	0,12
Helium dilution, dil	-5,11	10^{-5}
Use of lens, $lens$	0,41	0,34
Accuracy	89,1%	

Table 4.5: MLR results for the dependent variable pressure ratio.

ture equivalence ratio (p-value = 0,12) are slightly influent in the pressure ratio prediction. Conversely, helium dilution stands as the most statistically relevant variable (p-value = 10^{-5}). The regression model returned a mean relative error of 10,9%, which means an accuracy of 89,1%.

The regression equation for the dependent variable pressure ratio, which uses the coefficients θ_i seen in Table 4.5, is given by:

$$p_{ratio} = 7,01 + 0,20T_0 - 1,21p_0 - 1,37\phi - 5,11dil + 0,41lens \tag{4.4}$$

As stated before, pressure ratio is a continuous variable and hence the regression equation Eq. (4.4) returns a prediction for the pressure ratio likely to be obtained during the ignition. The intercept term (θ_i = 7,01) shows that, for the average experimental onset, the pressure ratio prediction is 6,83 without lens ($lens$ = 0 $\rightarrow$ p_{ratio} = 6,83) and 7,24 with lens ($lens$ = 1 $\rightarrow$ p_{ratio} = 7,24). The use of lens slightly increases the pressure ratio prediction, but as observed in Table 4.5, the independent variable $lens$ is poorly correlated with the pressure ratio (p-value = 0,34). Initial temperature (θ_i = 0,20), initial gas pressure (θ_i = -1,21) and equivalence ratio (θ_i = -1,37) are poorly correlated with pressure ratio. The mean increase produced in pressure ratio by an unitary increase of T_0 is 0,01 (ΔT_0 = 1ºC $\rightarrow$ Δp_{ratio} = 0,01), whereas an unitary rise in p_0 induces a decrease of -0,01 in pressure ratio (Δp_0 = 1 bar $\rightarrow$ Δp_{ratio} = 0,01) and an ϕ increase of 0,01 means a decrease of 0,12 ($\Delta\phi$ = 0,1 $\rightarrow$ Δp_{ratio} = -0,12). Unitary increases in helium dilution, which has been concluded as the most relevant independent variable, provokes a decrease in the pressure ratio prediction of 0,24 (Δdil = 0,01 $\rightarrow$ Δp_{ratio} = 0,24).

It can be concluded that dilution factor controls the strength of the ignition of the volatile H_2/O_2 mixture, and hence the pressure ratio obtained. As discussed in Castela 2017 [27], the pressure ratio around eight is the theoretical limit between deflagration and detonation. Being so, regressions for Detonation and pressure ratio should present similarities. Indeed, both are very similar; the initial temperature has opposite influence yet very small, but the rest of independent variables present the same symbols in the respective coefficients, which means same influences.

4.2.2 Neural Network

In this section, the results returned by the developed neural network for the dependent variable the pressure ratio are presented. The neural network was mainly designed for the dependent variable ignition regime prediction and, hence, it solves multiclass classification problems. Therefore, the variable pressure ratio, which is a continuous magnitude, will be transformed into a discrete variable. The continuum was divided into four intervals: [1, 5], [5, 8], [8, 10] and [10, 15]. This division separates deflagrations and detonations, since pressure ratio 8 is a threshold between both regimes, as stated in Castela 2017 [27]. The study of this frontier between deflagrations and detonations (p_{ratio} = 8) will add more awareness of the detonation ignition regimes.

The new discrete variable pressure ratio is represented in Fig. 4.5, where the intervals are assigned to an index value, namely: 1 for $p_{ratio} \in$ [1, 5]; 2 for $p_{ratio} \in$ [5, 8]; 3 for $p_{ratio} \in$ [8, 10]; 4 for $p_{ratio} \in$ [10, 15];

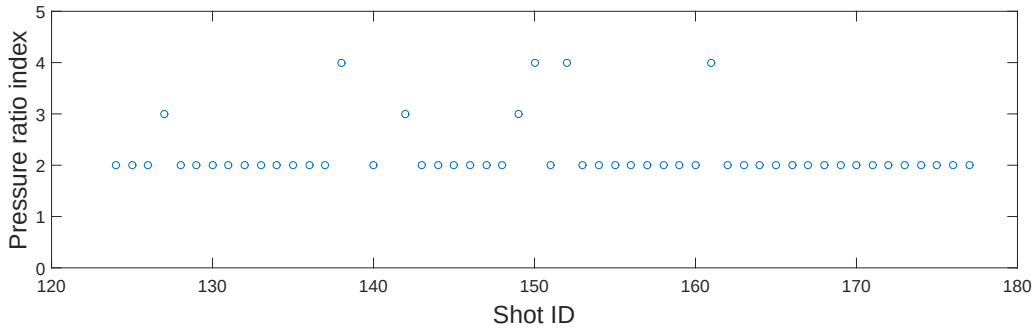

Figure 4.5: Discretization of the dependent variable pressure ratio.

Figure 4.5 shows the distribution of this new discrete variable. The first interval refers to extremely weak ignitions or the absence of ignition. Note that the index one is empty beacuse the two shots that did not trigger ignition were removed from the statistical study. However, most shots belong to the second or third intervals. Moreover, the fourth interval, including pressure ratios above ten, is considerably uncommon.

Therefore, the neural network returns the probability of certain experimental onset of returning a pressure ratio within each interval. The variation of each independent variable with respect the average experimental onset provides the graphs that allow the qualitative study of the pressure ratio. This procedure is the same than that seen in Section 4.1.2. As stated in Section 4.1.2, the use of lens correlates with the formation of detonations, so a previous analysis was not considerd necessary. Hence, the unitary influence of the rest of independent variables (initial temperature, initial gas pressure, equivalence ratio and helium dilution) are presented below.

Figures 4.6-4.9 show the probability distribution of each pressure ratio interval for the range of values of the independent variables (Initial temperature, initial gas pressure, equivalence ratio and helium dilution), for both ignition sources (withou lens and with lens).

- **Impact of the initial temperature, T_0.**

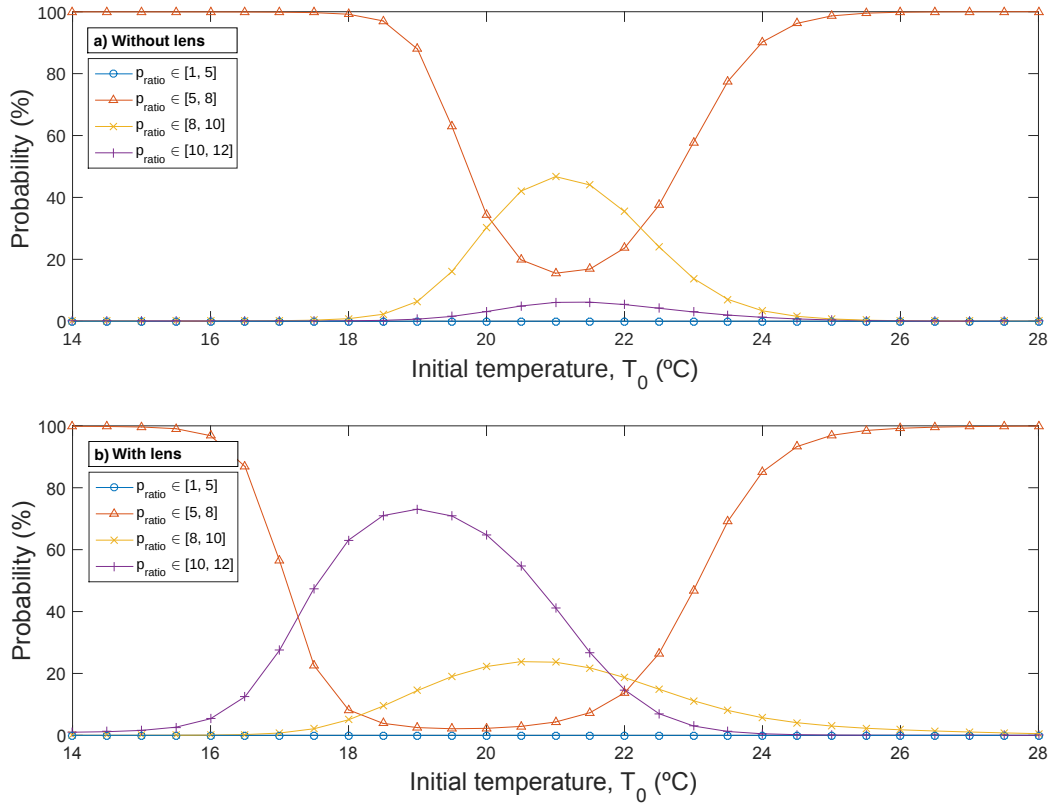

Figure 4.6: Pressure ratio probability distribution regarding T_0, conditioned by (a) without lens and (b) lens.

Figure 4.6a shows that, for most of the initial temperature range considered (from 14 to 28 ºC), the pressure ratio is likely to be within the interval of 5 and 8 with 100% if lens are not used, which means that deflagration would be the ignition regime to be triggered. However, the probability of this interval ($p_{ratio} \in$ [5, 8]) decreases from T_0 = 18 ºC to T_0 = 21 ºC, when it reaches its minimum of 15%. From that temperature value (21ºC), the probability of $p_{ratio} \in$ [5, 8] increases until reaching again 100%. This quadratic evolution is also followed by the probability of pressure ratio within the interval of 8 and 10 ($p_{ratio} \in$ [8, 10]). In fact, this probability increases from 0% to a value of 50%, and then monotonically decreases to 0%, in the same range of T_0 observed for the interval of pressure ratio [5, 8]. On the other hand, probability distributions with lens are observed in Fig. 4.6b. It shows the same quadratic evolution of probabilities observed in the case without lens, yet enhanced. For T_0 below 17 ºC and above 22 ºC, the pressure ratio is likely to be within the interval of 5 and 8. For the rest of inital temperature range, the pressure ratio is most likely to be within the interval [10, 12] with probabilities up to 75%. Hence, it can be concluded that, as seen in the analysis of the variable Ignition regime (Section 4.1.2), the optical configuration allows more energetic ignition. When using lens, the range of T_0 for p_{ratio} related with detonation events is wider (from 17 to 22 ºC), and the pressure ratio is also likely to be higher.

- **Impact of the initial gas pressure, p_0.**

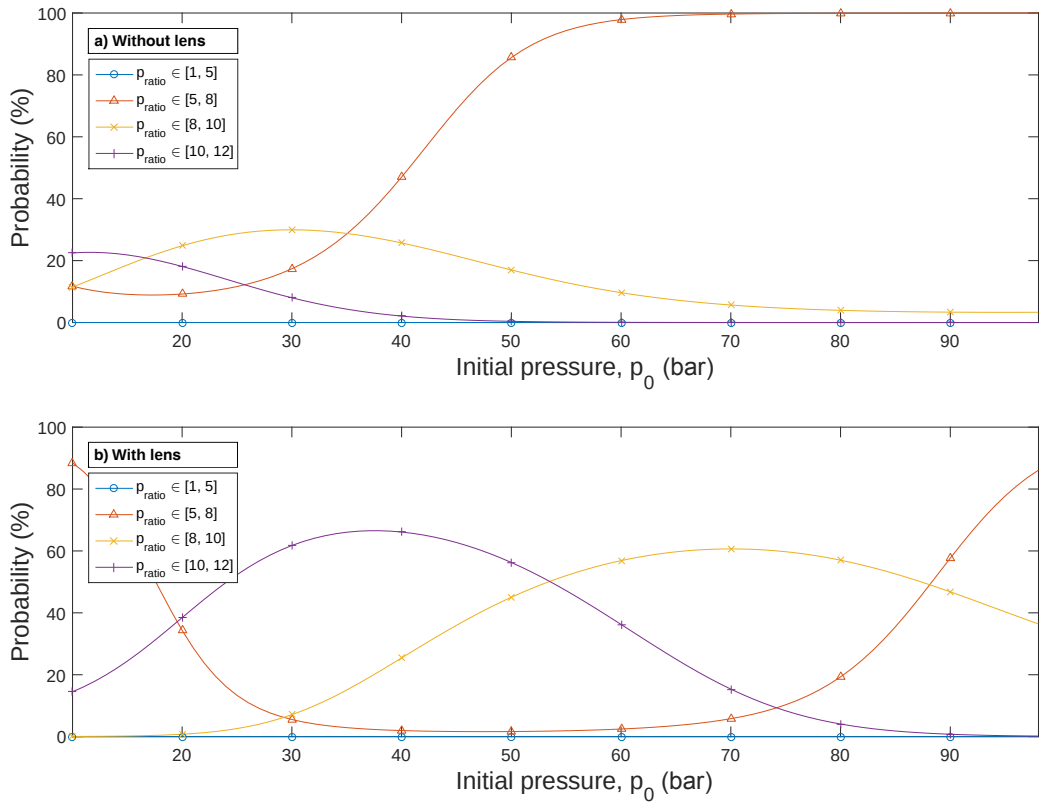

Figure 4.7: Pressure ratio probability distribution regarding p_0, conditioned by (a) without lens and (b) lens.

Figure 4.7a shows a poor probability distribution for $p_0 < 35$ bar. The statistical analysis is not conclusive for low pressures when lens are not used, as concluded in the analysis of ignition regime (Section 4.1.2). For $p_0 < 35$ bar, the probability of $p_{ratio} \in$ [5-8] has a monotonic increase from 35% to 100% at p_0 = 60 bar. For higher initial pressures, the probability distribution does not present changes. If lens are used to drive the shot ignition, probability distribution is considerably different, as seen in Fig. 4.7b. Using lens, intervals of p_{ratio} that involve detonations are likely to be predicted for the range of p_0 considered. Probability of p_{ratio} within the interval [10, 12] quadratically evolves around p_0 = 40 bar, where a maximum probability value of 70% is reached. On the other hand, the probability of $p_{ratio} \in$ [8, 10] follows the same pattern yet shifted to higher initial pressures. The maximum value of $p_{ratio} \in$ [8, 10] probability is in p_0 = 70 bar. In fact, it can be appreciated in Figs. 4.7a and 4.7b that the poor probability distribution observed in the case without lens for low inital pressures seems to be replicated in the case with lens, but enhanced and shifted to higher initial gas pressure values. It can be concluded from these results that the pressure ratio obtained in the ignition is correlated with the initial gas pressure p_0. Higher p_0 values induce lower p_{ratio} predictions, which agrees with the conclusion of the regression analysis with MLR.

- **Impact of the equivalence ratio, ϕ.**

Figure 4.8a shows a probability distribution similar to that observed in the pressure ratio proba-

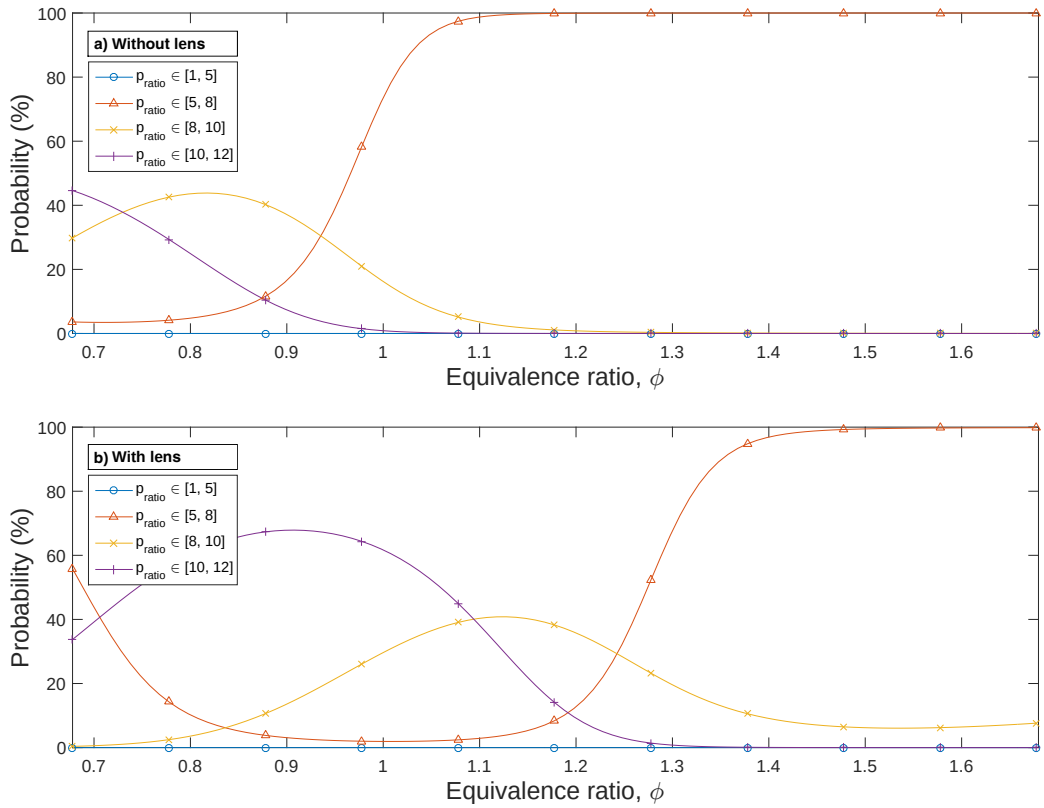

Figure 4.8: Pressure ratio probability distribution regarding ϕ, conditioned by (a) without lens and (b) lens.

bility distribution with initial gas pressure without laser, Fig. 4.7a. The graph shows a monotonic increase in probability of $p_{ratio} \in$ [5, 8], from 10% to 100%, for values of ϕ within the interval of 0,9 and 1,1. In fact, for $\phi >$ 0,95, pressure ratio is likely to be predicted within that interval [5, 8]. Conversely, for $\phi <$ 0,95, predictions shows pressure ratios within the interval [8, 10], with probabilities up to 45% for ϕ near 0,8. Unlike the analysis of Ignition regime showed (Section 4.1.2, no quadratic evolution is appreciated around the stoichiometric equivalence ratio (ϕ = 1) in Fig 4.8a. However, Fig. 4.8b shows a quadratic distribution around the vicinity of the equivalence ratio ϕ = 1 when lens are used. The probability distribution is considerably similar to the case without lens but shifted to higher equivalence ratios. The intervals involving detonation event ($p_{ratio} \in$ [8, 10] and $p_{ratio} \in$ [10, 12]) are most likely to predicted for $\phi <$ 1,2, with probabilities up to 70% (ϕ = 0,9). A monotonic rise in the probability of pressure ratio to be within the interval of 5 and 8 is observed for $\phi >$ 1,2, reaching 100% ($\phi >$ 1,4). As concluded in the analysis with MLR, high equivalence ratio values are likely to return lower pressure ratio, yet it is know from the analysis of ignition regime with Neural Networks that there is a quadratic evolution around near the stoichiometric equivalence ratio, which is seen only in the case with lens (Fig. 4.8b). As explained, the excess of either air/O_2 or fuel/H_2 absorbs part of the energy provided to trigger the ignition. It is concluded that the energy absorption is higher for rich mixtures (excess of fuel/H_2) than for lean mixtures (excess of air/O_2).

- **Impact of the helium dilution factor, dil.**

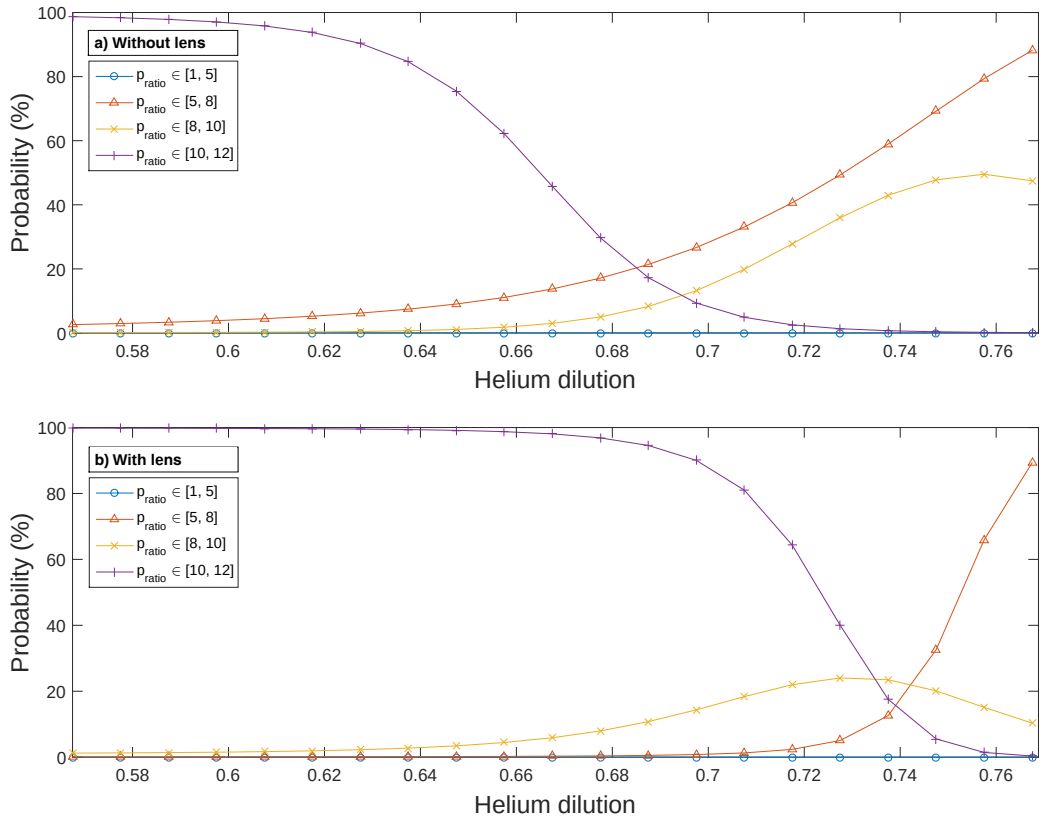

Figure 4.9: Pressure ratio probability distribution regarding dil, conditioned by (a) without lens and (b) lens.

As seen in the analysis of ignition regime with Neural Networks (Section 4.1.2), the probability distribution of pressure ratio with dilution factor, shown in Fig. 4.9, is different of those seen with the rest of independent variables. Figure 4.9a shows that for low values of helium dilution ($dil <$ 0,68), the pressure ratio is likely to be within the interval [10, 12], which means that the ignition regime would be detonation. This probability monotonically decreases from 100% at dil = 0,6 to 20% at dil = 0,68. From that dilution value, the deflagration-related pressure ratio interval, [5, 8] shows a monotonic increase to reach a probability of 90% at dil = 0,77, the highest dilution factor considered. These results are enhanced when the optical configuration of the experiment is changed and lens are engaged. As shown in Fig. 4.9b, for dilution values below the average value (dil = 0,72), the pressure ratio is likely to be within the interval [10, 12] with a 100% probability. This probability monotonically decreases for $dil >$ 0,68. As in the case without lens, for high dilution factors ($dil >$ 0,74), the interval [5, 8] is the most likely to be predicted; its probability rapidly increases from 10% to 90%. Evolution of pressure ratio probability distribution shows that, for both ignition sources (without lens and with lens), dil is the independent variable more correlated with the probability of detonation. This can be seen in the graphs presented along the analysis of the dependent variables ignition regime and pressure ratio with Neural Networks, and in the regression p-values shown in the analysis of these dependent variables with MLR.

In this section, the neural network has dealt with one variable ($_{ratio}$), whereas in Section 4.1.2 it had to deal with four regimes, modelled as dichotomous variables. Therefore, the expected accuracy in the predictions is higher. Indeed, the neural network returned an accuracy of 98%, which means that just one shot was mispredicted. This is a very satisfactory result, although the algorithm does not return a discrete value for the dependent variable pressure ratio. The matrices $\Theta^{(1)}$ and $\Theta^{(2)}$ used in this section are presented together with the matrices used in Section 4.1.2 in Appendix B.

4.3 Consumption velocity results

4.3.1 MLR

The consumption velocity is related with the strength of the ignition, so the statistical study can be useful for the final goal of the work. This dependent variable a continuous magnitude, such as pressure ratio, so Multivariate Linear Regression is applied to predict a non normalized value of this consumption velocity. The shot #150 (see Fig. 3.13), which supposed an anomaly in the consumption velocity records, was not taken into account in this MLR analysis. The omission of this particular pulse considerably increased the accuracy of the predictions, due to the linear character of the regression.

Table 4.6 shows the coefficients returned by the regression analysis of the variable consumption velocity.

	Consumption velocity coefficients		
Variable	θ_i		p-values
Intercept term	24,39	m/s	0,00
Initial temperature, T_0	6,93	m/s	0,37
Initial gas pressure, p_0	-44,37	m/s	10^{-5}
Equivalence ratio, ϕ	-27,53	m/s	0,01
Helium dilution, dil	-105,92	m/s	0,00
Use of lens, $lens$	-2,92	m/s	0,58
Accuracy	53,3%		

Table 4.6: MLR results for the dependent variable consumption velocity.

As stated in Table 4.6, the regression coefficients θ_i have velocity units, m/s, because consumption velocity is not normalized. The p-values shown in Table 4.6 reveal that the consumption velocity is the dependent variable more influenced by the experimental onset, from a statistical standpoint. Initial gas pressure (p-value = 10^{-5}), mixture equivalence ratio (p-value = 0,01) and helium dilution factor (p-value = 0,00) play a main role as predictors of the mixture consumption velocity. As seen in the pressure ratio regression analysis (see Table 4.5), low gas pressures, low equivalence ratios and low dilutions produce higher velocity of mixture consumption. The relation between these variables is clear, yet consumption velocity predictions returned way lower accuracy, just 53,3%.

The consumption velocity regression equation is given by Eq. (4.5).

$$v_{ch} = 24,39 + 6,93T_0 - 44,37p_0 - 27,53\phi - 105,92dil - 2,92lens \tag{4.5}$$

The average experimental onset returns a consumption velocity of 25,7 m/s without lens ($lens$ = 0 $\rightarrow$ v_{ch} = 25,7 m/s) and 22,8 m/s with lens ($lens$ = 1 $\rightarrow$ v_{ch} = 22,8 m/s). Initial temperature coefficient (θ_i = 6,93) induces a rise of 0,5 m/s if T_0 increases 1 ºC (ΔT_0 = 1 ºC $\rightarrow$ Δv_{ch} = 0,5 m/s). On the other hand, p_0, ϕ and dil are strongly correlated with the consumption velocity, as observed in their p-values (Table 4.6). An increase of 1 bar in p_0 means a mean decrease of 0,5 m/s in the consumption velocity (Δp_0 = 1 bar $\rightarrow$ Δv_{ch} = -0,5 m/s) and an unitary increase of ϕ causes a decrease of 2,5 m/s in the consumption velocity prediction ($\Delta\phi$ = 0,1 $\rightarrow$ Δv_{ch} = -2,5 m/s). Dilution factor also correlates with consumption velocity inversely. An increase of 0,01 in dil, while the rest of independent variables do not vary, means a decrease of 5,0 m/s in the consumption velocity (Δdil = 0,01 $\rightarrow$ Δv_{ch} = -5,0 m/s). Therefore, low initial pressure, low equivalence ratio and low dilution factor experimental onsets are likely to return high mixture consumption velocities.

The regression returned by the MLR analysis has the same influences as the pressure ratio regression, which matches the intuition about higher pressure ratios involving higher consumption velocities. The only difference remains in the feature lens, since the focalization of the laser leads to lower consumption velocities according to this model, whereas produced higher pressure ratios. This could be a link with the tulip flames formation, and therefore with dual slopes.

4.3.2 Neural Network

The dependent variable consumption velocity must be converted to discrete, or even dichotomous, in order to fit the neural network, which was created mainly to solve a multiclass classification problem. Such transformation was carried out in Section 4.2.2 because of the direct relevance of pressure ratio in the prediction of the regime obtained, due to the frontier existing between deflagration and detonation in the pressure ratio domain (p_{ratio} = 8). However, the relation between consumption velocity and regimes is not clear enough to perform a probability study with Neural Networks, such as the studies in Sections 4.1 and 4.2. Therefore, this dependent variable will not undergo the analysis offered by the neural network.

4.4 PCA

As explained along the document, PCA is to be used to reduce the dimensions of the problem, even when the supervised algorithms have proven that all five independent variables (initial temperature, initial gas pressure, equivalence ratio, helium dilution and use of lens) are statistically relevant. However, a new lower dimensional space can be used to look at the data from a brand new standpoint. Thus, the dimensional space of the combustion problem are reduced, allowing to plot the projected data in a 2D

graph. Moreover, K-means algorithm is implemented before this dimension reduction is applied in order to classify the ESTHER experiments regarding the experimental onset. This implementation aims to correlate the experimental onsets and the ignition regimes obtained in the experiments. Therefore, four clusters (one per ignition regime) are considered.

4.4.1 Dimension reduction

The reduction of the problem's dimensions is carried out steply until reaching the desired two dimensions. During the process, the variables are projected and eventually dissapear. However, when the dimension reduction has been performed, two of the independent variables will remained. The algorithm works selecting the variable that presents less deviance and projecting the rest of them onto it. This dimension reduction process is explained in details in Section 3.3.4.

After the dimension reduction, the variables mostly unchanged are identified as initial temperature and lens. Both original variable and the new projected variables are shown in Figs. 4.10 and 4.11.

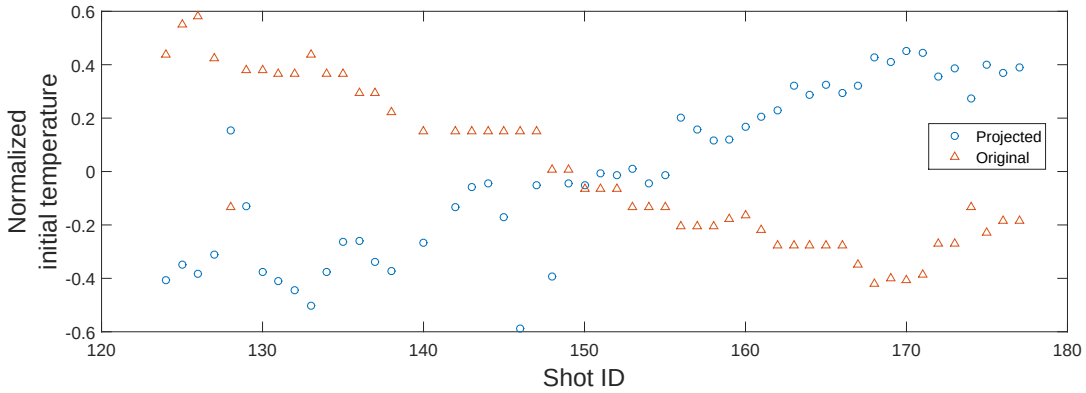

Figure 4.10: Comparison between the original initial temperature and the projected initial temperature.

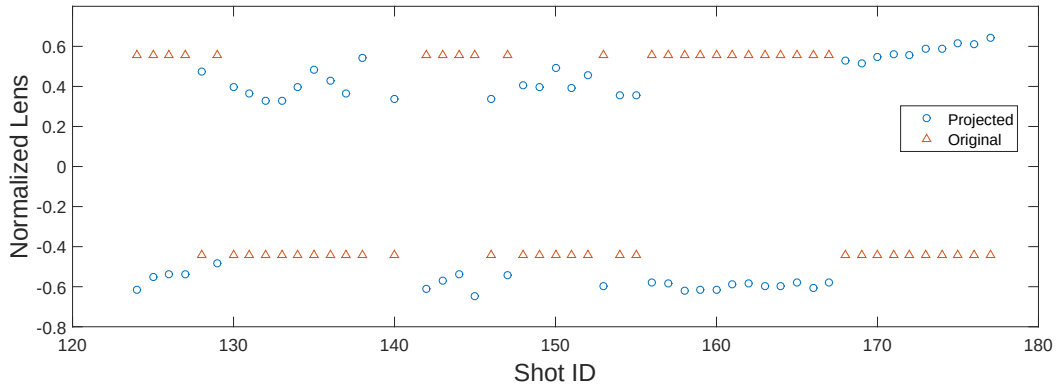

Figure 4.11: Comparison between the original lens and the projected lens.

As shown in Figs. 4.10 and 4.11, the two variables remained mainly unchanged yet inverted. During the projection process, the variables are inverted due to the first variable chosen to be reduced, helium dilution. This inversion has no effect in the performance of the algorithms since it exists proportionality

between the original and projected variables.

The dimensional space of the problem has been reduced to a bidimensional space. The two dimensions are represented in Fig. 4.12.

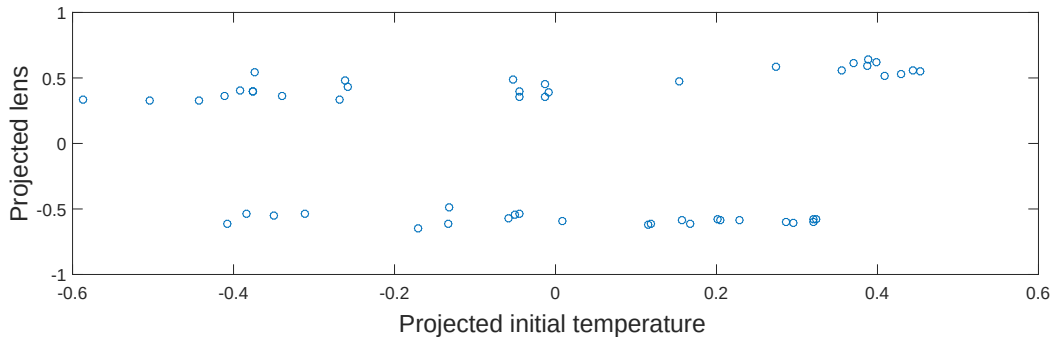

Figure 4.12: Reduction of the combustion dimensional space.

This representation in 2D provides an adequate environment to implement the K-means algorithm.

4.4.2 Data clustering

The clustering operation finds as many centroids within the sample as asked for by reducing the distance between the centroid and its assigned shots. Hence, at the end of the process every single shot is assigned to one of the four centroids. The goal is to check the existence of a correlation between these uninformed clusters and the four ignition regime categories. Once the assignment is complete, the shots will be projected again into a 2D plot, such as the one shown in Fig. 4.12.

It is important to note that the clustering is performed before the dimension reduction, so the simplicity of the two-dimensional problem does not affect the clustering. The results of the K-means algorithm implementation can be observed in Fig. 4.13.

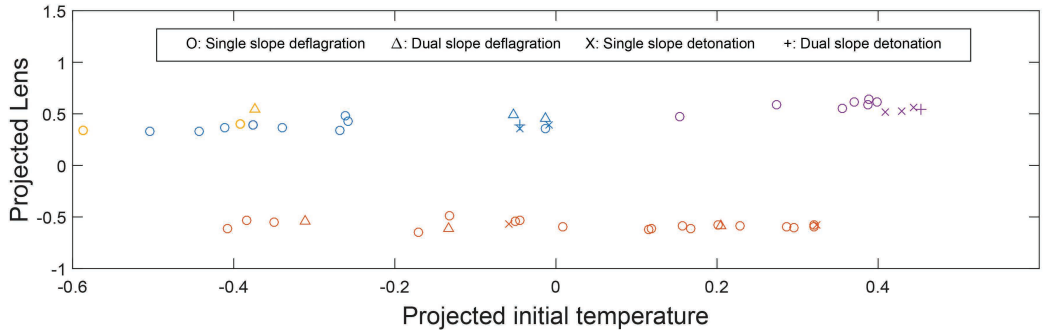

Figure 4.13: Data clusters found by the algorithm, differentiated by colors.

In Fig. 4.13, the different ignition regimes are set apart by the shape of the point, as stated in the legend of the figure. The color of the points represents the different clusters. As recommended by Ng [29], the K-means algorithm was run ten times in order to choose the most adequate clustering, which offers best centroids location. This experiment was repeated a couple of times, yet the algorithm always converged to the same result, shown in Fig. 4.13.

Figure 4.13 shows that one cluster englobes all shots that did not use lens. There is a cluster that has assigned just three shots, while the other two clusters distribute the rest of shots, all of them using lens in the ignition. The intended correlation is not obvious in the figure, as clusters do not correspond with regimes. Consequently, it can be concluded that the complexity of the problem makes two similar experimental onsets present completely different results.

The fact that independent variable Lens organizes these clusters reafirms its importance in the initial conditions. The greater number of clusters in the side corresponding with the experiments with lens may highlight that the use of lens lead to a wider variety of regimes than the abstence of lens. Indeed,the set of shots using focalized laser as ignition source presents more ignition regime variety than the set of shots that did not engage the lens. Indeed, some checking of the results provided by the neural network in the prediction of ignition regime shows that, whereas two out of four mispredicted shots are the two shots that returned dual slope detonation, the other two mispredicted shots used laser without lens as ignition source. In fact, further experiments show that unfocalized laser shots are mispredicted more often, which confirms what PCA revealed. The poor ignition regime distribution in the sample of ESTHER shots mainly affects to the set of experiments carried out without lens, which are more likely to return single slope deflagration ignition regime.

Chapter 5

Conclusions

Two different supervised algorithms, MLR and Neural Networks, have been used to understand and determine the detonation regime in ESTHER driver section. Besides, PCA, used along with the K-means algorithm, has complemented the investigation with unsupervised statistical data.

Analysis with MLR has provided a regression equation for each dependent variable: Detonation, Dual Slope, pressure ratio and consumption velocity. These regression equations have been discussed along Chapter 4. In fact, the accuracy given by these regression models shows that MLR is a simple yet powerful tool for combustion regimes predictions.

The results mentioned above are reinforced by the results of the Neural Networks analysis. The neural network has built a precise map of weights after its training with the shots database. The larger this database is, the more accurate will be the predictions, as it will have more information to model the combustion. The graphs provided as results of the Neural Networks analysis can be used as guideline to empiracally predict the different outcomes of the ESTHER combustion.

Regarding the independent variables considered for the combustion determination, the following conclusions were extracted:

- Initial temperature, an independent variable that was suspected of being non influential, has been proven to be relevant in the propagation of the flame front and tulip flames formation. However, its correlation with detonation regimes is really weak within the range of temperatures operated by ESTHER shock-tube.

- The initial gas pressure has been found not to be as relevant in the regime obtained after the shot as was firstly thought. It has moderate influence in the pressure ratio obtained, and it finds its strongest correlation with the consumption velocity. Both initial temperature and initial gas pressure, have opposite influences in pressure ratio and consumption velocity prediction, which makes us think that the gas mixture density could be a key factor in the propagation of the flame front and, hence, the formation of dual slope pressure-time curves.

- The equivalence ratio of the mixture is also important in the detonation process. Although the linear character of MLR shows a negative influence (so lean mixtures would produce higher detonation probabilities) the results provided by the neural network have shown that the influence of this independent variable is, indeed, non linear. The combustion efficiency reaches its maximum with the stoichiometric H_2/O_2 mixture and slightly richer mixtures. Higher combustion efficiency means that increases in pressure and temperature are achieved in the chamber after ignition.

- Both MLR and Neural Networks concluded that dilution is a key factor in the outcome of the combustion. The explosive behavior of the H_2/O_2 mixture makes helium completely necessary, since it has been proven that low helium dilution factors automatically lead to detonation. This dilution is, statistically speaking, the most important variable for detonation formation, as well as for the consumption velocity and the pressure peak achieved.

- Regarding the ignition source, the lens used to focalize the laser into a single point drastically changes the behavior of the combustion. The sharper temperature gradient induced often leads to instabillity and turbulence, which causes strong deflagration and detonations. The interaction between laser and the reactive gas mixture is still to be fully understood under extreme conditions. Yet, the statistical analysis has revealed that the focalized mode triggers detonation easily. Also, the ignition source is strongly related with the formation of tulip flames, taking into account that the initial temperature gradient determines the first stadiums in the development of the flame.

The dependent variables (Ignition regime, pressure ratio and consumption velocity) have been found related among them. Higher pressure peaks during the ignition involve higher consumption velocities and more powerful ignitions and detonations. The pressure-times curves displayed in this manuscript present much more noise in the signal recovered when detonation occurs, which remarks the violent and chaotic behavior inherent to the turbulence of detonation regimes. Moreover, dual slope has been found to be a really solid regime in different situations.

PCA was used along with the K-means algorithm to reduce the dimensional space of the problem. This reduction was unfruitful because of the preliminary analysis carried out in Section 3.2.2. However, the use of PCA confirmed that two similar experimental onsets lead to very different regimes, due to the instability and difficult repeatability of ESTHER combustion. Otherwise, the trained clusters would have correlated with ignition regimes. PCA also showed that the variety of experimental onsets is greater in shots driven with lens and, therefore, their predictions are consequently more accurate. It also remarked the neccesity of a more diverse database for experiments without lens.

The multi-physics that drive ESTHER shock-tube combustion have been studied using statistical methods, which returned large data about the different interactions between the variables involved in the combustion and its possible outcome. This data provides the first step into the understanding of such a complex process and improvements has been achieved in this analysis.

5.1 Future Work

The neural network is a very complex algorithm, yet the one used in this manuscript was relatively simple. Efforts towards a more complex network would involve the determination of its optimal structure.

The study of more variables in the combustion, such as focus point of the laser in 3D, vessel dimensions, ambient humidity or gas density, can lead to interesting results. With enough variables, PCA could been properly used, and its reduced dimensions would feed the neural network, which could be at the same time linked to several MLR algorithms or even other neural networks. Interaction between machine learning algorithms is a field yet to be applied in combustion, but it could lead to very interesting results for the development of new technologies.

Further research about ESTHER's multi-physics combustion involves the implementation of the prediction methods in the experiments, so the algorithms are fed with a shot once it has been done. In this way, the growth of the sample will increase the accuracy of the models. It would also involve the gathering of most shots returning detonation, dual slope and the combination of them, in order to fully determine a map of coefficients that fits the whole sample.

Lastly, the ongoing investigations will lead to the completion of ESTHER project. The laser combustion studied in ESTHER shock-tube will serve the future of engineering and space exploration, as intended by the European Space Agency, ESA.

Bibliography

[1] H. D. Ng, Y. Ju, and J. H. S. Lee. Assessment of detonation hazards in high-pressure hydrogen storage from chemical sensitivity analysis. *International Journal of Hydrogen Energy*, 32(1):93–99, January 2007. 10.1016/j.ijhydene.2006.03.012.

[2] G. Ciccarelli, T. Ginsberg, J. Boccio, and C. Economos. Detonation cell size measurements and predictions in hydrogen-air-steam mixtures at elevated temperatures. *Combustion and Flame*, 99 (2):212–220, November 1994. 10.1016/0010-2180(94)90124-4.

[3] T. Kratzel, E. Pantow, and H. Eichert. Modelling of hydrogen combustion: Turbulent flame acceleration and detonation. *International Journal of Hydrogen Energy*, 21(5):407–414, May 1996. 10.1016/0360-3199(95)00099-2.

[4] J. Jarosinski and B. Veyssiere. *Combustion Phenomena: Selected Mechanisms of Flame Formation, Propagation, and Extinction*, chapter Instability Phenomena during Flame Propagation, pages 93–100. CRC Press Books, 2009.

[5] H. Xiao, J. Sun, and P. Chen. Experimental and numerical study of premixed hydrogen/air flame propagating in a combustion chamber. *Journal of Hazardous Materials*, 268:132–139, January 2014. 10.1016/j.jhazmat.2013.12.060.

[6] J. Li, Z. Zhao, A. Kazakov, and F. L. Dryer. An updated comprehensive kinetic model of hydrogen combustion. *International Journal of Chemical Kinetics*, 36:566–575, 2004.

[7] R. Albalak, A. R. Frisancho, and G. J. Keeler. Domestic biomass fuel combustion and chronic bronchitis in two rural bolivian villages. *Thorax*, 54:1004–1008, 1999.

[8] J. Bennett, V. Krishnamoorthy, S. Liu, R. Grout, E. Hawkes, J. Chen, V. Pascucci, and P. T. Bremer. Feature-based statistical analysis of combustion simulation data. *IEEEI Transactions on Visualization and Computer Graphics*, November 2011.

[9] M. L. Traver, R. J. Atkinson, and C. M. Atkinson. Neural network-based diesel engine emissions prediction using in-cylinder combustion pressure. *SAE Technical Paper Series*, May 1999.

[10] A. Tailor, D. Jurkovic, T. H. Bourne, W. P. Collins, and S. Campbell. Sonographic prediction of malignancy in adnexal masses using multivariate logistic regression analysis. *Ultrasound Obstet. Gynecol.*, 10:41–47, 1997.

[11] A. A. A. Alsharif and B. Pradhan. Urban sprawl analysis of tripoli metropolitan city (Libya) using remote sensing data and multivariate logistic regression model. *Journal of the Indian Society of Remote Sensing*, 42(1):149–163, March 2014.

[12] M. Meng and D. Niu. Modeling CO_2 emissions from fossil fuel combustion using the logistic equation. *Energy*, 36(5):3355–3359, May 2011. 10.1016/j.energy.2011.03.032.

[13] Z. Wang, C. Song, and T. Chen. Deep learning based monitoring of furnace combustion state and measurement of heat release rate. *Energy*, 131(15):106–112, July 2017. 10.1016/j.energy.2017.05.012.

[14] H. A. Rowley, S. Baluja, and T. Kanade. Rotation invariant neural network-based face detection. In *Computer Vision and Pattern Recognition, 1998. Proceedings. 1998 IEEE Computer Society Conference on*, pages 38–44. IEEE, 1998.

[15] Z. Chuan, L. Xianliang, H. Mengshu, and Z. Xu. A LVQ-based neural network anti-spam email approach. *ACM SIGOPS Operating Systems Preview*, 39(1):34–39, 2005.

[16] G. J. Tesauro, J. O. Kephart, and G. B. Sorkin. Neural networks for computer virus recognition. *IEEE Expert*, 11(4):5–6, August 1996. 10.1109/64.511768.

[17] D. A. Pomerleau. Efficient training of artificial neural networks for autonomous navigation. *Neural Computation*, 3(1):88–97, 1991. 10.1162/neco.1991.3.1.88.

[18] E. Tosun, K. Aydin, and M. Bilgili. Comparison of linear regression and artificial neural network model of a diesel engine fueled with biodiesel-alcohol mixtures. *Alexandria Engineering Journal*, 55(4):3081–3089, December 2016. 10.1016/j.aej.2016.08.011.

[19] R. Pino-Mejías, A. Pérez-Fargallo, C. Rubio-Bellido, and J. A. Pulido-Arcas. Comparison of linear regression and artificial neural networks models to predict heating and cooling energy demand, energy consumption and CO_2 emissions. *Energy*, 118(1):24–36, January 2017. 10.1016/j.energy.2016.12.022.

[20] A. Vaughan and S. V. Bohac. Real-time, adaptive machine learning for non-stationary, near chaotic gasoline engine combustion time series. *Neural Networks*, 70:18–26, October 2015. 10.1016/j.neunet.2015.04.007.

[21] F. Perini. High-dimensional, unsupervised cell clustering for computationally efficient engine simulations with detailed combustion chemistry. *Fuel*, 106:344–356, April 2013. 10.1016/j.fuel.2012.11.015.

[22] J. C. Shuterland and A. Parente. Combustion modeling using principal component analysis. *Proceedings of the Combustion Institute*, 32(1):1563–1570, 2009. 10.1016/j.proci.2008.06.147.

[23] B. J. Isaac, J. N. Thornock, J. Shuterland, P. J. Smith, and A. Parente. Advanced regression methods for combustion modelling using principal components. *Combustion and Flame*, 162(6): 2592–2601, June 2015. 10.1016/j.combustflame.2015.03.008.

[24] H. Mirgolbabaei and T. Echekki. A novel principal component analysis-based acceleration scheme for LES–ODT: An a priori study. *Combustion and Flame*, 160(5):898–908, May 2013. 10.1016/j.combustflame.2013.01.007.

[25] O. Owoyele and T. Echekki. Toward computationally efficient combustion dns with complex fuels via principal component transport. *Combustion Theory and Modelling*, 21(4):770–798, March 2017. 10.1080/13647830.2017.1296976.

[26] M. L. da Silva, B. B. de Carvalho, A. Smith, and L. Marraffa. High-pressure H_2/He/O_2 combustion experiments for the design of the ESTHER shock-tube driver. *46th AIAA Thermophysics Conference*, pages 2016–4156, June 2016.

[27] M. L. Castela, M. Levy, M. L. da Silva, B. B. de Carvalho, A. Smith, and L. Marraffa. Ignition of H_2/O_2/He mixtures in a high-pressure (up to 50 bar) bomb vessel. *8th European Combustion Meeting*, April 2017.

[28] D. Dunn-Rankin and R. Sawyer. Tulip flames: changes in shape of premixed flames propagating in closed tubes. *Experiments in Fluids*, 24(2):130–140, February 1998. 10.1007/s003480050160.

[29] A. Ng. Machine Learning. Coursera.

Appendix A

H_2/O_2 reaction mechanism

The combustion model menctioned in Chapter 2, which belongs to the work of Li *et al.* [6], is exposed in the following pages.

Table I. Detailed H_2/O_2 Reaction Mechanism. Units are cm^3-mol-sec-kcal-K, and $k = A\,T^n \exp(-E/RT)$.

			A	n	E	Reference
H_2/O_2 Chain Reactions						
1.	$H + O_2 = O + OH$		3.55×10^{15}	-0.41	16.6	Hessler [16]
2.	$O + H_2 = H + OH$		5.08×10^{4}	2.67	6.29	Sutherland et al. [44]
3.	$H_2 + OH = H_2O + H$		2.16×10^{8}	1.51	3.43	Michael et al. [45]
4.	$O + H_2O = OH + OH$		2.97×10^{6}	2.02	13.4	Sutherland et al. [46]
H_2/O_2 Dissociation/Recombination Reactions						
5.	$H_2 + M = H + H + M$ [a]		4.58×10^{19}	-1.40	104.38	Tsang et al. [47]
	$H_2 + Ar = H + H + Ar$		5.84×10^{18}	-1.10	104.38	Tsang et al. [47]
	$H_2 + He = H + H + He$		5.84×10^{18}	-1.10	104.38	See text
6.	$O + O + M = O_2 + M$ [a]		6.16×10^{15}	-0.50	0.00	Tsang et al. [47]
	$O + O + Ar = O_2 + Ar$		1.89×10^{13}	0.00	-1.79	Tsang et al. [47]
	$O + O + He = O_2 + He$		1.89×10^{13}	0.00	-1.79	See text
7.	$O + H + M = OH + M$ [a]		4.71×10^{18}	-1.0	0.00	Tsang et al. [47]
8.	$H + OH + M = H_2O + M$ [b]		3.8×10^{22}	-2.00	0.00	See text
Formation and Consumption of HO_2						
9.	$H + O_2 + M = HO_2 + M$ [c]	k_O	6.37×10^{20}	-1.72	0.52	Michael et al. [19] (M = N_2)
	$H + O_2 + M = HO_2 + M$ [d]	k_O	9.04×10^{19}	-1.50	0.49	Michael et al. [19] (M = Ar or He)
		k_∞	1.48×10^{12}	0.60	0.00	Cobos et al. [48]
10.	$HO_2 + H = H_2 + O_2$		1.66×10^{13}	0.00	0.82	Mueller et al. [1]
11.	$HO_2 + H = OH + OH$		7.08×10^{13}	0.00	0.30	Mueller et al. [1]
12.	$HO_2 + O = OH + O_2$		3.25×10^{13}	0.00	0.00	Baulch et al. [34]
13.	$HO_2 + OH = H_2O + O_2$		2.89×10^{13}	0.00	-0.50	Baulch et al. [34]
Formation and Consumption of H_2O_2						
14.	$HO_2 + HO_2 = H_2O_2 + O_2$ [e]		4.20×10^{14}	0.00	11.98	Hippler et al. [49]
	$HO_2 + HO_2 = H_2O_2 + O_2$		1.30×10^{11}	0.00	-1.63	
15.	$H_2O_2 + M = OH + OH + M$ [f]	k_O	1.20×10^{17}	0.00	45.5	Warnatz [50]
		k_∞	2.95×10^{14}	0.00	48.4	Brouwer et al. [51]
16.	$H_2O_2 + H = H_2O + OH$		2.41×10^{13}	0.00	3.97	Tsang et al. [47]
17.	$H_2O_2 + H = H_2 + HO_2$		4.82×10^{13}	0.00	7.95	Tsang et al. [47]
18.	$H_2O_2 + O = OH + HO_2$		9.55×10^{6}	2.00	3.97	Tsang et al. [47]
19.	$H_2O_2 + OH = H_2O + HO_2$ [e]		1.00×10^{12}	0.00	0.00	Hippler et al. [52]
	$H_2O_2 + OH = H_2O + HO_2$		5.8×10^{14}	0.00	9.56	

[a]Efficiency factors are: $\varepsilon_{H2O} = 12.0$, $\varepsilon_{H2} = 2.5$, $\varepsilon_{Ar} = 0.75$, and $\varepsilon_{He} = 0.75$. When a rate constant is declared specifically for Ar or He collision partner, the efficiency of Ar or He is set to zero when determining M for the same reaction.

[b]Efficiency factors are: $\varepsilon_{H2O} = 12.0$, $\varepsilon_{H2} = 2.5$, $\varepsilon_{Ar} = 0.38$, and $\varepsilon_{He} = 0.38$.

[c]When the main bath gas is N_2. Troe parameter is: $F_c = 0.8$. Efficiency factors are: $\varepsilon_{H2O} = 11.0$, $\varepsilon_{H2} = 2.0$, and $\varepsilon_{O2} = 0.78$.

[d]When the main bath gas is Ar or He. Troe parameter is: $F_c = 0.5$. Efficiency factors are: $\varepsilon_{H2O} = 16.0$, $\varepsilon_{H2} = 3.0$, $\varepsilon_{O2} = 1.1$, and $\varepsilon_{He} = 1.2$.
[e]Reactions 14 and 19 are expressed as the sum of the two rate expressions.
[f]Troe parameter is: $F_c = 0.5$. Efficiency factors are: $\varepsilon_{H2O} = 12.0$, $\varepsilon_{H2} = 2.5$, $\varepsilon_{Ar} = 0.64$, and $\varepsilon_{He} = 0.64$.

Appendix B

Weights matrices used in Chapter 4

In Sections 4.1.2 and 4.2.2, Chapter 4, results proposed are based in a specific pairs of weights/coefficients matrices $\Theta^{(1)}$ and $\Theta^{(2)}$. These matrices did return satisfactory predictions, so it is consider useful to include them in the document.

Due to the large number of decimals provided by MATLAB, the matrices in this Appendix were round to the third significant decimal.

B.1 Ignition regime matrices

Matrix $\Theta^{(1)}$, which involves the input and hidden layers of the neural network, is given by Table B.1.

$\Theta^{(1)}$	$\Theta_{i1}^{(1)}$	$\Theta_{i2}^{(1)}$	$\Theta_{i3}^{(1)}$	$\Theta_{i4}^{(1)}$	$\Theta_{i5}^{(1)}$	$\Theta_{i6}^{(1)}$
$\Theta_{1j}^{(1)}$	2,072	4,275	3,404	-0,107	2,642	4,577
$\Theta_{2j}^{(1)}$	-0,634	-7,209	2,293	5,628	3,226	-2,750
$\Theta_{3j}^{(1)}$	-2,574	-3,934	-7,677	7,233	1,880	0,145
$\Theta_{4j}^{(1)}$	2,264	-5,704	3,564	7,031	-3,890	-1,686
$\Theta_{5j}^{(1)}$	0,747	-6,662	-2,273	5,936	7,474	1,293
$\Theta_{6j}^{(1)}$	1,534	-3,708	-3,011	2,087	-4,710	3,344
$\Theta_{7j}^{(1)}$	0,346	0,455	0,190	-0,217	-1,868	1,876

Table B.1: Weight matrix $\Theta^{(1)}$ used in Section 4.1.

It is important to note that each column of matrix $\Theta^{(1)}$ is related with one of the variables considered, namely intercept term, initial temperature, initial gas pressure, equivalence ratio, helium dilution and use of lens.

The second weights matrix $\Theta^{(2)}$, which involves the hidden and output layers, is given by Table B.4.

Regarding this second matrix $\Theta^{(2)}$, each row is related with each one the possible ignition regimes, i.e. single slope deflagration, dual slope deflagration, single slope detonation and dual slope detonation respectively.

$\Theta^{(2)}$	$\Theta_{i1}^{(2)}$	$\Theta_{i2}^{(2)}$	$\Theta_{i3}^{(2)}$	$\Theta_{i4}^{(2)}$	$\Theta_{i5}^{(2)}$	$\Theta_{i6}^{(2)}$ $\Theta_{i7}^{(2)}$	$\Theta_{i8}^{(2)}$	
$\Theta_{1j}^{(2)}$	2,864	6,094	5,095	8,653	-4,914	-6,980	-4,070	0,400
$\Theta_{2j}^{(2)}$	-2,185	-4,084	0,896	-5,983	-2,730	6,912	3,148	-1,280
$\Theta_{3j}^{(2)}$	-7,252	-1,965	-7,301	-2,691	7,988	0,155	3,785	1,522
$\Theta_{4j}^{(2)}$	-3,062	-0,777	0,570	-3,754	0,439	4,758	-3,122	-2,112

Table B.2: Weight matrix $\Theta^{(2)}$ used in Section 4.1.

B.2 Pressure ratio matrices

Matrix $\Theta^{(1)}$, which involves the input and hidden layers of the neural network, is given by Table B.3.

$\Theta^{(1)}$	$\Theta_{i1}^{(1)}$	$\Theta_{i2}^{(1)}$	$\Theta_{i3}^{(1)}$	$\Theta_{i4}^{(1)}$	$\Theta_{i5}^{(1)}$	$\Theta_{i6}^{(1)}$
$\Theta_{1j}^{(1)}$	-0,119	-4,700	-1,251	-3,824	-4,608	1,991
$\Theta_{2j}^{(1)}$	2,011	15,034	-5,286	-9,761	-0,481	2,456
$\Theta_{3j}^{(1)}$	-3,475	8,996	-8,829	-7,519	9,218	2,271
$\Theta_{4j}^{(1)}$	1,978	-1,079	-2,229	-1,952	1,028	-2,275
$\Theta_{5j}^{(1)}$	0,346	1,318	1,943	0,672	4,168	-0,251
$\Theta_{6j}^{(1)}$	-0,346	-1,318	-1,943	-0,672	-4,168	0,251
$\Theta_{7j}^{(1)}$	-4,402	10,329	0,489	3,918	1,348	-5,162

Table B.3: Weight matrix $\Theta^{(1)}$ used in Section 4.2.

As stated before, each column of matrix $\Theta^{(1)}$ is related with one of the variables considered: intercept term, initial temperature, initial gas pressure, equivalence ratio, helium dilution and use of lens; respectively.

The second weights matrix $\Theta^{(2)}$, which involves the hidden and output layers, is given by Table B.4.

$\Theta^{(2)}$	$\Theta_{i1}^{(2)}$	$\Theta_{i2}^{(2)}$	$\Theta_{i3}^{(2)}$	$\Theta_{i4}^{(2)}$	$\Theta_{i5}^{(2)}$	$\Theta_{i6}^{(2)}$ $\Theta_{i7}^{(2)}$	$\Theta_{i8}^{(2)}$	
$\Theta_{1j}^{(2)}$	-19,461	0,000	0,000	0,000	0,000	0,000	0,000	0,000
$\Theta_{2j}^{(2)}$	5,001	0,967	-12,730	11,693	2,138	2,073	-2,073	7,529
$\Theta_{3j}^{(2)}$	-1,866	-5,753	7,336	-8,418	-2,668	3,018	-3,018	-8,197
$\Theta_{4j}^{(2)}$	-10,720	4,937	8,892	-7,690	0,511	-3,643	3,643	-1,233

Table B.4: Weight matrix $\Theta^{(2)}$ used in Section 4.2.

The rows in this matrix $\Theta^{(2)}$ correlate with the different intervals in which the variable pressure ratio was divided in (see Fig. 4.5, in Section 4.2.2). Although most coefficients in the first row appear as zero, they are not, yet first the significant figure belongs in the fifth decimal or further.